Atmospheric
Chemistry
and Physics

Measurement report: Inland ship emissions and their contribution to NO_x and ultrafine particle concentrations at the Rhine

Philipp Eger[1,★]**, Theresa Mathes**[1,a,★]**, Alex Zavarsky**[1]**, and Lars Duester**[1]

[1]Qualitative Hydrology, Federal Institute of Hydrology, Koblenz, Germany
[a]now at: Environmental Chemistry and Air Research, Technische Universität Berlin, Berlin, Germany
★These authors contributed equally to this work.

Correspondence: Philipp Eger (eger@bafg.de) and Theresa Mathes (mathes@tu-berlin.de)

Abstract. Emission plumes of around 4700 ship passages were detected between March 2021 and June 2022 in the Upper Rhine Valley in Worms, Germany. In combination with ship-related data recorded via the automatic identification system (AIS), the plume composition of individuals ships was analyzed, and it was possible to quantify their contribution to the overall emission load. To obtain an integral picture of inland ship emissions, nitrogen oxide ($NO_x = NO + NO_2$) and carbon dioxide (CO_2) measurements in the gas phase were combined with detailed particle-phase measurements including particle number concentration (PNC), particle size distribution (PSD) from 5 nm to 10 µm, particulate matter (PM_1 and $PM_{2.5}$), ultrafine particle fraction (UFP, diameter < 100 nm) and aerosol black carbon (BC). One measuring station was located inside a bridge directly above the navigation channel and was especially helpful in deriving emission factors under real-world driving conditions for the fleet on the Upper Rhine. The other station was situated on a riverbank at about 40 m distance to the shipping lane and was thus representative of the exposure of people working or living close to the Rhine. Inland ships contributed 1.2 µg m^{-3} or 7 % on average to the local nitrogen dioxide (NO_2) concentration at the bridge above the shipping lane. NO_x concentrations were increased by 10.5 µg m^{-3} (50 %), PNC by 800 cm^{-3} (10 %), PM_1 by 0.4 µg m^{-3} (4 %) and BC by 0.15 µg m^{-3} (15 %). On the riverbank a NO_x increase of 1.6 µg m^{-3} (8 %) and an NO_2 increase of 0.4 µg m^{-3} (3 %) were observed. More than 75 % of emitted particles were found in the UFP range with a geometric mean particle diameter of 52 ± 23 nm. Calculated emission factors (25–75 percentiles) were 26–44 g kg^{-1} of fuel for NO_x, 1.9–3.2 g kg^{-1} for NO_2, 0.3–0.7 g kg^{-1} for BC, 0.9–2.3 g kg^{-1} for PM_1 and $(1-3) \times 10^{15}$ kg^{-1} for PNC, with a large variability observed from ship to ship. Relating these values to ship-specific parameters revealed the importance of engine characteristics, i.e., vessels using old motors with low revolutions per minute (rpm) caused comparably high emission factors for both NO_x and PNC. A comparison with emission regulation limits set by the Central Commission for the Navigation of the Rhine (CCNR) and the European Union (EU) showed that – within the uncertainty of our calculation method – mean energy-dependent emission factors under real-driving conditions were slightly exceeding those under controlled laboratory conditions. The results from this study underline the importance of long-term measurements with high temporal resolution to reliably estimate the contribution of inland shipping to air pollution in cities along heavy traffic waterways and to monitor a potential future emission reduction when modernizing the fleet.

1   Introduction

Shipping is a potential contributor to air pollution in coastal regions, harbors and along inland waterways with high traffic density (Eyring et al., 2010; Viana et al., 2014; Karl et al., 2019; Tang et al., 2020; Fink et al., 2023). In western Europe, where a large number of goods are transported on rivers and canals, inland ships can increase nitrogen oxides ($NO_x = NO + NO_2$), particulate matter (PM), aerosol black carbon (BC) and ultrafine particle (UFP) concentrations on a local scale (Uherek et al., 2010; Van der Gon and Hulskotte, 2010; Keuken et al., 2014; Kurtenbach et al., 2016; Pohl et al., 2017; Krause et al., 2023). In particular the Rhine as Europe's most important waterway in terms of transport volume is of major significance as it connects densely populated cities where people are often exposed to air pollution from road transport, industry and residential heating (Uherek et al., 2010; WHO, 2021). In Germany around 50×10^9 tkm (tonnekilometer) of goods per year is transported by inland vessels, which makes it the EU country with the highest transport performance in this sector, closely followed by the Netherlands (CCNR, 2021). Commonly inland navigation is considered the most environmentally friendly mode of transport in terms of the volume of freight moved (Federal Ministry for Digital and Transport, 2019), and that is why the European Commission aims to strengthen the role of inland waterway transport and increase the volume of goods transported on waterways by 50 % (European Commission, 2021). This consideration highlights the urgent need to better understand, and therefore more extensively monitor, the impact of ship emissions on air quality.

In recent years pollution from road traffic and seagoing ships and the negative impact of particulate matter on human health have become the subject of a vital scientific discussion (WHO, 2021; Sokhi et al., 2022), but there are only a few measurement studies dealing with European inland shipping in particular (van der Zee et al., 2012; Kurtenbach et al., 2016; Pohl et al., 2017; Kattner, 2019; Krause et al., 2023). Most of them took place at a fixed location for a short period of time or only concentrated on one specific compound. The only long-term study so far has been conducted in Duisburg at the Lower Rhine within the scope of the European research project "Clean Inland Shipping" (CLINSH) (Krause et al., 2023) where emission factors for NO_x were reported and compared to onboard measurements directly at the exhaust line. Particulate matter and especially UFP from inland vessels have been investigated in more detail solely by Pohl et al. (2017), although the World Health Organization (WHO) recommends the measurement of this particle size range and its integration into existing air quality monitoring (WHO, 2021). The difficulty here is that emitted UFPs are variable in their size and number concentration and can be affected by nucleation, condensation and coagulation processes, resulting in a strong dependence on wind conditions, plume age, and distance between emitter and measurement location (Ce-

lik et al., 2020). Apart from the limited number of onshore and a few onboard (Schweighofer and Blaauw, 2009; Pillot et al., 2016) measurements, several modeling studies and emission inventories are available (Van der Gon and Hulskotte, 2010; Knörr et al., 2013; Korsten, 2018) which are, however, subject to uncertainties arising from inevitable assumptions made and from the use of generalized emission factors.

The impact of seagoing ships (and non-European inland ships) on air quality in coastal and port areas has been more frequently investigated (Moldanová et al., 2009; Jonsson et al., 2011; Diesch et al., 2013; Alföldy et al., 2013; Beecken et al., 2014, 2015; Buffaloe et al., 2014; Pirjola et al., 2014; Seyler et al., 2017; Cao et al., 2018; Celik et al., 2020; Jiang et al., 2021; Kuittinen et al., 2021; Schwarzkopf et al., 2022), but due to different fuel types (especially the higher sulfur content) and ship dimensions the results are not transferable to inland ships. Permanent measurement stations that monitor air quality in the EU are usually located in cities near busy roads with a focus on road traffic. Although these stations are useful to check compliance with emission regulations for NO_2, $PM_{2.5}$ and PM_{10} (European Union, 2008), they do not provide a deeper insight into the share of different emission sources (including road traffic, industry, agriculture, residential heating and shipping). In particular the distinction between emissions from inland vessels and diesel-powered vehicles is difficult as they use the same fuel (apart from colorants and additives), for which a maximum sulfur content of 0.001 % is allowed in Germany (10. BImSchV., 2010). In contrast to road traffic, inland vessels are generally older and emission regulations (especially for NO_x and PM) are only valid for newly registered motors from 2003 on (CCNR, 2022; overview given in Table S1 in the Supplement). With the introduction of the Euro V stage in 2020 (European Union, 2016) emission limits for NO_x and PM have been tightened, but due to grandfathering and long motor lifecycles, the initiated transition to a low-emission inland fleet is slow.

Despite the growing relevance of inland shipping and because of the difficulty of using the abovementioned existing monitoring networks, there is a critical lack of emission measurements for inland ships under real-driving conditions. We show that from measured ship plumes and position data from the automatic identification system (AIS), emission factors (relative to the amount of fuel used) for several pollutants as well as the fractional contribution from ship traffic can reliably be derived. The presented dataset combines gas-phase (NO_x and CO_2) with particle-phase (PM, BC, UFP and particle size distribution) measurements and delivers an integrative overview on the impact of inland vessels on air quality for the river Rhine. The wide measured particle size range of 5 nm to 10 µm, the high temporal resolution of ~ 1 s and a measurement period of more than 1 year provide a novel insight into particulate emissions from inland shipping. An essential part was the application of a fast mobility particle sizer (FMPS) measuring the whole size distribution in paral-
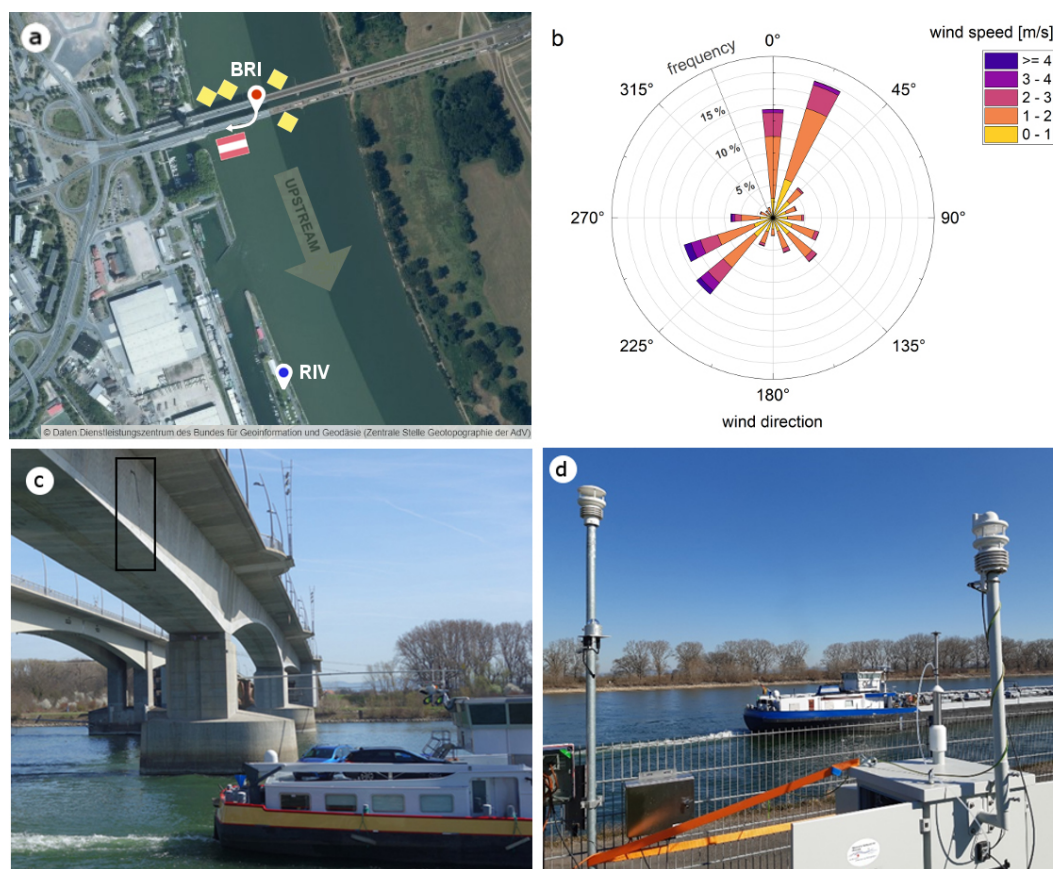
Figure 1. **(a)** Satellite image with measurement station inside the bridge (BRI) and station on the riverbank (RIV). Data: © GeoBasis-DE/BKG (2023). Ships traveling upstream preferably used the western shipping lane (yellow diamond means passage allowed, two yellow diamonds mean passage recommended), whereas ships traveling downstream were forced to the eastern shipping lane (red–white–red flag means passage forbidden). **(b)** Wind rose for the whole measurement period. **(c)** Setup at BRI with sampling line framed in black. **(d)** Setup at RIV.

lel by the use of numerous electrometers. For the detection of short-term increases like ship plumes it has a crucial advantage over commonly used scanning mobility particle sizers (SMPSs) which need several tens of seconds for a scan and thus depend on the size spectrum not changing significantly over time. Emission factors representative of the fleet operating on the Upper Rhine section between Mannheim and Mainz and their dependence on ship parameters (e.g., motor power and revolutions per minute, rpm) were derived from the dataset and offer the potential for the enhancement of emission inventories and transport models.

2 Methods

2.1 Measurement site

Measurements were carried out at two stations along the Upper Rhine (Rhine kilometer 444) in Worms, Germany, over a period of more than 1 year (March 2021 to August 2021 and November 2021 to June 2022). The city of Worms is located on the west side of the river Rhine, whereas on the east

side the landscape is dominated by rural structures including agricultural areas, as indicated in Fig. 1a. Meteorological conditions varied throughout the year but were mainly characterized by northern and southwestern winds (Fig. 1b).

One station was located inside the Nibelungen bridge (labeled BRI, Fig. 1c) at a mean height of ~ 10 m above the shipping lane (depending on water level) where ships were traveling upstream (further referred to as upstream ships), at a distance of 40 m to the western riverbank. The instruments were located in a room inside the bridge which provided protection from rain, high humidity and rapid temperature fluctuations. Instrument-specific sampling lines of 4–5 m length were led through a hole in the wall and downwards to a point sharply below the edge of the bridge's base to reduce the impact of turbulence on the incoming flow. In this way, the distance to the traffic lane on the bridge was also increased to ~ 6 m so that the impact of traffic emissions on the measurement site was minimized. For a period of 2 months, the sampling inlet was also moved to the lane where ships were traveling downstream (downstream ships) at 100 m dis-

tance to the western riverbank. The other station was located about 500 m upstream from the bridge on the riverbank (labeled RIV, Fig. 1d) at a distance of 40 m and 100 m to the shipping lanes. Here the instruments were placed inside an air-conditioned container (25 °C), with sampling lines of approximately 1 m length for the gas-phase measurements and a customized sampling head for the particle-phase measurements.

The two stations were chosen to be as close as possible to the shipping lane to enable plume identification but at sufficient distance to the city center to avoid strong interferences from road traffic. Occasionally we observed an increased atmospheric variability in the NO_x signal that probably originated from local non-ship sources like road traffic (favored in the presence of thermal inversions). These periods were, however, excluded from the analysis by defining appropriate criteria in the peak-finding algorithm (see Sect. 2.3.1), so that the results were not biased. BRI was primarily set up to derive emission factors with a minimum uncertainty since the point of measurement is very close to the emission source. RIV was installed in February 2022 to monitor pollutant emissions at a more representative location in order to compare them with local background levels. At RIV the signal was strongly dependent on the predominant wind direction with noticeable signals found for northeasterly winds, whereas at BRI ship plumes were detected mostly independently from wind conditions, although with varying magnitude.

2.2 Instruments

Table 1 lists the instruments used to measure CO_2, NO_x, particle number concentration (PNC), particle size distribution (PSD), particulate matter (PM) concentration and black carbon (BC). In order to capture the shape of the ship plumes in real time, all instruments were operated at the highest possible temporal resolution (1 to 6 s).

2.2.1 Trace gas measurements

CO_2 was measured by non-dispersive infrared spectroscopy (NDIR) with an LI-850 device (LI-COR Biosciences) and a temporal resolution of 1 s. For the combined measurement of NO_2 and NO_x an ICAD instrument (Airyx) based on the iterative cavity-enhanced DOAS method (Horbanski et al., 2019) was applied. It simultaneously measured NO_2 and NO_x at a high temporal resolution of ~ 2 s and contained an integrated CO_2 sensor (FlowEvo) serving as an additional CO_2 measurement (correlation with LI-COR device: slope $= 0.94$, $R^2 = 0.97$; see Fig. S1 in the Supplement). Parallel NO_x measurements at RIV were carried out with the NO_x analyzer model 405 (2B Technologies, 5 s temporal resolution) which directly measures NO_2 via absorption at 405 nm and NO by converting it to NO_2 via gas-phase titration (Birks et al., 2018). O_3 was monitored via absorption

spectroscopy with the ozone monitor model 205 (2B Technologies). For the gas-phase instruments we used perfluoroalkoxy (PFA) tubing with 4 mm inner diameter (i.d.) and 6.35 mm outer diameter (o.d.). The residence time in the sampling lines was on the order of 1–2 s so that no significant losses to surfaces are expected for the gases measured in this study. The instrument performance was checked on a regular basis (zero and span tests). For NO, NO_2 and O_3 this was done via the calibrator model 714 (2B Technologies) with a user-adjustable output of the three gases and an NO_2 permeation source. For CO_2 a gas bottle with a mixing ratio of 2000 ppm and a reservoir of soda lime as a zero-air reference were used.

2.2.2 Particle measurements

PNC and PSD from 6 to 520 nm diameter were detected in 16 size channels by a fast (electric) mobility particle sizer spectrometer (TSI, FMPS 3091) with a frequency of 1 Hz. Particles ranging from 0.25 to 2.5 μm diameter were captured optically by an aerosol spectrometer (Grimm, 11-D) with a time resolution of 1 s. During the first weeks the size range was extended to 32 μm diameter (in 6 s mode), but no significant increase in coarse mode particles > 2.5 μm was observed in ship plumes at BRI. This finding was confirmed by parallel measurements with a similar optical particle counter (Grimm, EDM 180) at RIV. Consequently, further measurements with the 11-D were only carried out up to 2.5 μm diameter to gain a higher temporal resolution.

For all particle measurement devices, particulate matter concentration (PM_1, $PM_{2.5}$) was derived from the PNC in the corresponding channels, assuming a constant density of 1.7 g cm^{-3}. This estimate is based on numerous literature studies on diesel exhaust and urban aerosols (Barone et al., 2011; Celik et al., 2020; Wang et al., 2021), also considering the relatively large BC fraction (~ 2 g cm^{-3}) measured in our study. Nevertheless, the number is subject to a substantial uncertainty as the exact particle composition is unknown and also changes over time. From the measured PSD the mode diameter (D_{mode}) and the geometric mean diameter (GMD) were determined. To measure BC an Aethalometer (Magee Scientific, AE33) with a time resolution of 1 s was used. The BC mass concentration is derived from the measurement of absorbance at 880 nm and real-time compensation of the filter loading effect (Drinovec et al., 2015). The fractional contribution from biomass burning can be derived from the difference in absorption at 470 and 880 nm. The AE33 was operated with a 2.5 μm cyclone to be in line with the optical particle measurement. For the particle-phase measurements 3 mm i.d. stainless steel tubing (Grimm 11-D) and conductive silicon tubing with 7.87 mm (FMPS) and 6.35 mm (AE33) i.d. were used. Transmission losses were calculated using the particle loss calculator tool (von der Weiden et al., 2009; see Fig. S2) and resulted in overall losses smaller than 10 % for all three instruments and particle diam-

Table 1. Instruments applied at BRI and RIV and their specifications.

Instrument	Variables	Time resolution	Precision[a] (1σ)	Accuracy[b]	Size range	BRI[c]	RIV[c]
LI-850 (LI-COR)	CO_2	1 s	0.3 ppm	1.5 %	–	x	x
ICAD (Airyx)	NO_2, NO_x CO_2	2 s	0.4 ppb 1.0 ppm		–	x	(x)
Model 405 (2B)	NO_2, NO_x	5 s	4.0 ppb	2.0 %	–		x
Model 205 (2B)	O_3	2 s	1.0 ppb	2.0 %	–	x	
FMPS 3091 (TSI)	PNC, $PM_{0.1}$, $PM_{0.5}$, size distribution	1 s			6–520 nm	x	
11-D (Grimm)	PNC, PM_1, $PM_{2.5}$, size distribution	1 s (6 s)			0.25–2.5 µm (0.25–32 µm)	x	
EDM 180 (Grimm)	PNC, PM_1, $PM_{2.5}$, size distribution	6 s			0.25–32 µm		x
SMPS + C (Grimm)	PNC, size distribution	85 s per scan			5–350 nm		x
AE33 (Magee)	BC	1 s	0.4 µg m^{-3}		0–2.5 µm	x	
AIS receiver (Watcheye R)	Ship position data and characteristics	10 s			–	x	x
Weather station[d] (Lufft)	T, RH, wind speed, direction, precipitation, global radiation	10 min			–		x

[a] The precision is derived from noise in our measurements at a constant representative concentration and highest possible time resolution. [b] Specified by the manufacturer.
[c] Columns indicate at which station the instruments were operated: x signifies full time and (x) partial time. [d] Temperature T and relative humidity RH.

eters up to 2.5 µm. A comparison between the Grimm 11-D at BRI (long tubing) and the EDM 180 at RIV (dedicated inlet system) confirmed these small particle losses.

2.2.3 Meteorological and AIS data

A permanent weather station in the city center (~ 10 m above the ground, operated by the Landesamt für Umwelt Rheinland-Pfalz) at ~ 1 km distance to BRI provided meteorological data throughout the whole measurement period. From February 2022 on this was complemented by a weather sensor directly located at RIV (Lufft/OTT HydroMet, WS700-UMB), measuring temperature (T), relative humidity (RH), wind speed, wind direction, precipitation intensity and global radiation. In general, both stations were in good agreement with respect to the prevailing wind direction (although wind speed and relative humidity were higher on the riverbanks).

Ship information and position data were recorded in a pseudonymized form using an AIS receiver (Watcheye R) and a program written in Python code. The Rhine in Worms is frequented by approximately 100 ships per day, which are mainly cargo (37 %) and tanker ships (35 %) but also a few passenger boats (4 %) and vessels of other type (not further specified or incorrectly assigned). The speed of the vessel rel-

ative to the river current (further referred to as speed through water, STW) was derived from the speed over ground (SOG) recorded via AIS and the flow velocity of the Rhine via SOBEK model data at 1 d resolution (Hydrokontor, 2014) (see Fig. S3). On average, upstream ships traveled at a SOG of 2.8 ± 0.4 m s^{-1} and downstream ships at 4.8 ± 0.7 m s^{-1}. Correcting for the velocity of the Rhine (~ 1.3 m s^{-1} on average), STW yielded 4.1 and 3.6 m s^{-1}, i.e., upstream ships were operated at a slightly higher engine load. The loading status can theoretically be derived from the AIS data as well but is not considered sufficiently reliable as it lies within the responsibility of the ship owner to keep the information up-to-date. The CCNR (2018) reports that vessels transporting mineral oil products (tankers) on the Upper Rhine are on average more heavily loaded when traveling upstream, whereas for sand and construction materials (cargo) the situation is reversed.

A database with additional technical vessel information for Rhine ships (mainly about the engine) was provided by the IVR (International Association for the Representation of the Mutual Interests of the Inland Shipping and the Insurance and for Keeping the Register of Inland Vessels in Europe) and processed in a pseudonymized form to comply with data protection guidelines. For the fleet operating on the Upper

Rhine in Worms we calculated a median age of the ships' main engine of 12 years (25–75 percentiles: 4–17 years), but the result might potentially be biased by the fact that newer motors are more likely to be listed in the database than older ones.

2.3 Data analysis

2.3.1 Peak identification and ship assignment

Data from gas- and particle-phase instruments were combined with the AIS dataset to identify potential peaks from passing ships. From the AIS position data (transmitted every 10 s) the point in time with the smallest distance to the point of measurement was determined and further used as a reference (t_0). In the next step the atmospheric background was calculated for each measured parameter using a low-pass filtered time series in the form of a running median with 10 min window size. By subtracting this value from the raw signal (see Fig. 2), most of the background variability (stemming from chemical and meteorological processes in the atmosphere and non-ship emission sources) was removed from the dataset, and only distinct peaks with a short duration of typically several tens of seconds remained. In the second step an algorithm was applied to automatically identify potential ship peaks by defining several criteria to be fulfilled, illustrated in Fig. 2.

i. A minimum number of three consecutive data points above a pre-defined threshold are chosen, which is defined as 4 times the standard deviation (σ) of the signal in a 30 s window before the potential peak start (t_{start}).

ii. A minimum peak height is chosen to avoid atmospheric variability or noise being interpreted as a ship peak.

iii. Peaks occurring in periods with high atmospheric variability were skipped when a precise separation from the background was impossible.

iv. The peak end (t_{end}) was defined as the point in time after which the signal decreased below the threshold level for more than 20 s.

v. The peak duration was limited to $\tau = 240$ s since longer peaks indicated an unusual maneuver (e.g., a turn).

Descriptive examples and further information can be found in the Supplement (Tables S2 and S3 and Fig. S4). If all criteria were fulfilled, peak duration, peak maximum, cumulative peak area and time of occurrence were stored. By using the peak area instead of the maximum value, biases from different measurement frequencies of the instruments were avoided. In the second step the peaks were assigned to passing ships if the following criteria were met:

vi. The peak was observed within the interval $\Delta t = -30$ to $+120$ s relative to the ship passage that is defined via
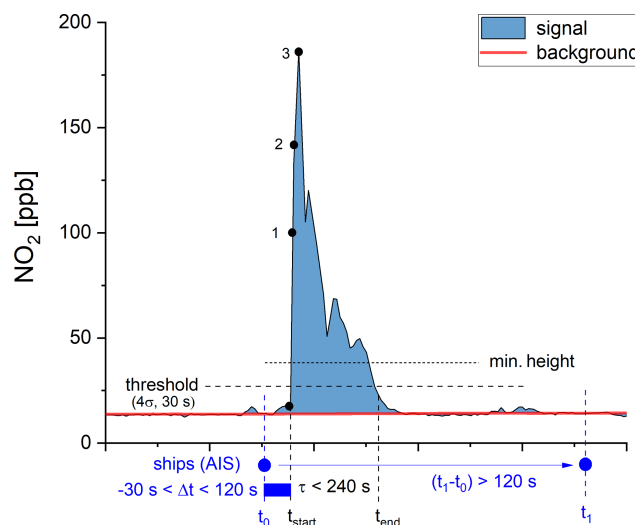

Figure 2. Exemplary peak illustrating the criteria applied for peak identification and ship assignment explained in Sect. 2.3.1.

the AIS position closest to the measurement station (expanded to -60 to $+240$ s at RIV).

vii. If more than one ship was present within a time span of 120 s (240 s at RIV), the corresponding peaks were rejected from the analysis, as a clear attribution to one single ship was impossible.

The remaining peaks provided the basis for the calculation of specific emission factors and the additional contribution from inland shipping.

2.3.2 Additional contribution from shipping

The average contribution from inland shipping to the overall emission load was calculated from the sum of all peaks that could be clearly attributed to a single ship passage (see criteria in Sect. 2.3.1) relative to the observed background value within a particular measurement period. This approach represents a lower-limit estimate, since a non-negligible number of peaks is excluded from the analysis (e.g., periods with ship traffic density that is too high or increased atmospheric variability), but prevents the results from being biased by peak-like structures from non-ship sources.

2.3.3 Emission factors

For each peak that was successfully assigned to a ship passage the emission factor E_X of a pollutant X (expressed in g of X per kg of fuel used) was derived from Eq. (1a). Here C_X is the peak area of pollutant X, C_{CO_2} the peak area of CO_2 (expressed in ppb s and ppm s), M_X the molar mass of X (46 g mol^{-1} for NO_2 and NO_x) and $M_{CO_2} = 44$ g mol^{-1} the molar mass of CO_2. Furthermore, the amount of CO_2 emitted per kilogram of burned fuel is estimated as $f_1 = 3150$ g kg^{-1},

assuming a carbon content in diesel fuel of 86 wt % (weight percent) C and complete combustion to CO_2 (Cooper, 2001; Kurtenbach et al., 2016). For particulate matter (PM) and number concentration (PNC) the emission factors were derived from Eqs. (1b) and (1c), with C_{PM} being the peak area of PM (expressed in $\mu g\,m^{-3}\,s$), C_{PNC} the peak area of PNC (expressed in cm^{-3}) and $V_{air} = 24.45\,L\,mol^{-1}$ the molar volume of air (at 25 °C and 1013 hPa).

$$E_X\left[g\,kg^{-1}\right] = f_1 \times \left(\frac{C_X}{C_{CO_2}}\right) \times \left(\frac{M_X}{M_{CO_2}}\right) \tag{1a}$$

$$E_{PM}\left[g\,kg^{-1}\right] = f_1 \times \left(\frac{C_{PM}}{C_{CO_2}}\right) \times \left(\frac{V_{air}}{M_{CO_2}}\right) \tag{1b}$$

$$E_{PNC}\,[kg^{-1}] = f_1 \times \left(\frac{C_{PNC}}{C_{CO_2}}\right) \times \left(\frac{V_{air}}{M_{CO_2}}\right) \tag{1c}$$

For Eqs. (1a)–(1c) to be valid we assume that pollutant X and CO_2 are diluted in a similar manner during transport from the point of emission to the point of measurement. This is a reasonable assumption for most components (NO_x, BC, PNC) as the plume age is on the order of seconds to a few minutes and mixing ratios will be conserved. The only exception is NO which is rapidly converted to NO_2 in the presence of O_3. Thus, the results for NO_2 were corrected for the amount of NO_2 that has been produced during plume transport. To calculate the initial concentration at the time of emission (Eq. 2), the amount of O_3 that has been consumed by the reaction with NO ((C_{O3})$_{decrease}$) was subtracted from the measured NO_2 signal ((C_{NO_2})$_{measured}$), resulting in a somewhat lower concentration of NO_2 at the time of emission ((C_{NO_2})$_{initial}$), while NO_x is conserved. The initial NO_2-to-NO_x ratio is then defined by Eq. (3).

$$\left(C_{NO_2}\right)_{initial} = \left(C_{NO_2}\right)_{measured} - \left(C_{O_3}\right)_{decrease} \tag{2}$$

$$\left(\frac{NO_2}{NO_x}\right)_{initial} = \frac{\left(C_{NO_2}\right)_{initial}}{\left(C_{NO_x}\right)_{measured}} \tag{3}$$

Emission factors were calculated separately for each measured component. As part of the quality check, emission factors were only considered reliable if for CO_2 and the analyte of interest the peak duration did not differ by more than a factor 3 and the time of occurrence of the peak maximum did not deviate by more than 20 s. The application of these quality control criteria helped in minimizing outliers and systematic uncertainties in the dataset. An exemplary plausibility check was carried out for data from December 2021 ($\sim$ 500 peaks); i.e., peaks considered unreliable ($< 4\%$) were manually removed from the dataset. The analysis revealed that both mean emission factors and the mean contribution from shipping hardly changed ($< 2\%$) when applying the additional manual filtering procedure. In addition, missing peaks in BC were checked in detail to decide whether the peak was just not automatically recognized or if there was really no BC or only a negligible amount present (e.g., due to applied particle filtering technology). In the latter case, which was true for $\sim 5\%$

of all ship plumes, the BC peak area was integrated manually (resulting in a value close to zero). In this way all the non-BC or very weak BC emitters were included in the statistics as well, which led to a marginal reduction in the calculated mean emission factor resulting from the automatic peak-finding routine.

For comparison with emission regulations the emission factor in grams per kilogram was transformed into an energy-related emission factor (expressed in g per kWh) using Eq. (4) and a specific fuel consumption reported for inland ships of $f_2 = 0.22\,kg\,kWh^{-1}$ (Federal Ministry for Digital and Transport, 2020), which is based on an analysis of inland vessel engine test-bed reports within a performance range of 25 % to 100 % of nominal power.

$$E'_X\left[g\,kWh^{-1}\right] = E_X\left[g\,kg^{-1}\right] \times f_2 \tag{4}$$

Although the fuel consumption in reality is not independent of driving conditions as the efficiency decreases at lower loads, the variability when traveling under typical operating conditions (like those observed in Worms) is very small.

2.3.4 Dependence on ship parameters and cluster analysis

The division of vessels into ship classes according to their length and width followed a CEMT scheme (CEMT, 1992) adjusted by Krause et al. (2023). Individual ships were further classified with respect to length, width, engine power, rpm and motor age using a k-means clustering algorithm. After (min–max) normalization of the data, clustering was performed separately for the NO_x and particle dataset. A number of $k = 5$ clusters was found to provide the most reliable results.

3 Results and discussion

3.1 General overview

Emission plumes of inland ships consist of a mixture of gaseous and particulate compounds, from which CO_2, NO, NO_2, PNC, PM_1, $PM_{2.5}$ and BC were analyzed in this study. For the two measurement stations in Worms (BRI and RIV) a total of 30 883 ship passages from 1781 different vessels were registered via AIS at BRI (10 703 passages from 1314 ships at RIV). Following the procedure described in Sect. 2.3.1, a fraction of $\sim 13\%$ (4060 peaks from 1181 ships) could be clearly attributed to a single ship passage at BRI (680 peaks from 476 ships at RIV). This relatively low yield arises from meteorological conditions and strict criteria set for the peak assignment algorithm. These criteria were necessary to avoid biases by false peak assignment but still provided a sufficiently large and representative sample. A 1 day example for BRI is shown in Fig. 3 where ship plumes are clearly visible as distinct spikes of various magnitudes and shapes and a drop in O_3.
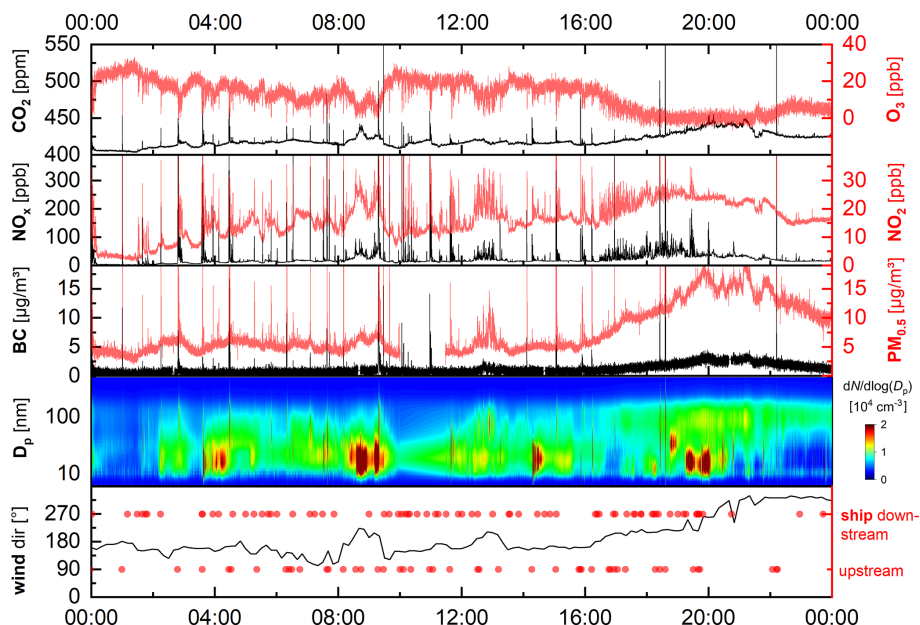
Figure 3. Exemplary time series for CO_2, O_3, NO_x, NO_2, BC, $PM_{0.5}$ (in this study similar to PM_1 and $PM_{2.5}$) and $dN/dlog(D_p)$ with number concentration N, particle diameter D_p, wind direction and ship traveling direction at BRI for 10 December 2021.

3.1.1   Nitrogen oxides (NO_x)

At BRI upstream ships caused median NO_x and NO_2 peak heights of 1053 ppb and 91 ppb, respectively, with observed maxima of 7851 and 3444 ppb (based on $N_{NO_x} = 2912$ and $N_{NO_2} = 3034$ peaks). These relatively large short-term peak values can be explained by the choice of the inlet location situated directly above the shipping lane. For downstream ships the relative peak height was a factor of 2–3 lower ($N_{NO_x} = 288$ and $N_{NO_2} = 306$) as they traveled with higher SOG resulting in a lower emission density along the track. At RIV median concentration peaks of 186 ppb NO_x and 37 ppb NO_2 and maxima of 3480 and 160 ppb were registered ($N_{NO_x} = 614$ and $N_{NO_2} = 531$). As diesel engines mainly emit NO, a median NO_2-to-NO_x ratio of 0.11 was observed at BRI. The initial ratio at the point of emission (see Sect. 2.3.3) was determined as 0.07, which is in good agreement with the ratio derived by Kurtenbach et al. (2016) for inland ships on the Lower Rhine. This value is also typical for diesel engines without exhaust gas aftertreatment systems, assumed to constitute the largest portion of the inland fleet (see Sect. 2.2.3). The use of catalysts and diesel particulate filters (DPFs) usually results in a somewhat higher ratio of 0.25–0.30 (Kurtenbach et al., 2016), whereas selective catalytic reduction (SCR) technology decreases it to 0.01. Applied to marine engines SCR and DPF were found to efficiently reduce NO_x and PM emissions by up to 90 % (Nuszkowski et al., 2009; Gysel et al., 2016; Sugrue et al., 2022). At RIV, emission plumes had more time to chemically react in the atmosphere before reaching the sampling inlet. As a consequence, more NO was converted to NO_2, and

the NO_2-to-NO_x ratio increased to 0.19. For further analysis only the initial NO_2 concentration was used, as the measured NO_2 in the plume was strongly dependent on the transport time and was not characteristic for a particular ship.

3.1.2   Particles (PNC, PSD, PM, BC)

The analysis of the PSD showed almost no particles in the coarse mode (2.5 to 10 µm diameter) present in ship plumes. The majority of emitted particles belonged to the ultrafine particle fraction (UFP, < 100 nm) with a fractional contribution of 76 ± 16 % relative to the total number of particles observed from 6 nm to 2.5 µm and 18 ± 20 % relative to the total particle mass. Since the FMPS (size range 6–520 nm) covered on average > 99.9 % of all particles detected in ship plumes, further results of PNC, PM_1 and $PM_{2.5}$ at BRI were based on this instrument.

Like for NO_x, the peak height values of PNC for downstream vessels were on average 2–5 times lower than for upstream vessels with an observed mean of $(0.6 \pm 1.4) \times 10^6$ cm^{-3} for PNC ($N_{PNC} = 1503$) and 323 ± 417 µg m^{-3} for PM_1 ($N_{PM} = 1503$). The mean peak area of upstream vessels amounted to 2710 ± 3192 µg m^{-3} s with a mean peak duration of 72 ± 52 s. A similar picture was obtained for BC, where peak height values of upstream vessels of 54 ± 65 µg m^{-3} ($N_{BC} = 1620$) were around 5 times higher than for downstream vessels. These results are consistent with a measurement study by Pohl et al. (2017) at the Lower Rhine. The high variability in our dataset can be explained by differences in meteorological conditions, ship position relative to the measurement station and vessel characteristics and is also in line

Table 2. Monthly averaged contribution from shipping at both measurement stations at the Rhine in Worms.

Analyte	Monthly additional contribution at BRI	N_{peaks}^a	Relative contribution	Monthly additional contribution at RIV	N_{peaks}	Relative contribution
CO_2	0.7–1.4 mg m^{-3}	3204	0.1 %–0.2 %	0.07–0.13 mg m^{-3}	1083	~ 0.01 %
NO_x	6.9–14.3 µg m^{-3}	4013	24 %–68 %	1.0–2.2 µg m^{-3}	1806	6 %–11 %
NO_2	0.7–1.6 µg m^{-3}	4607	3 %–10 %	0.3–0.5 µg m^{-3}	2374	2 %–4 %
BC	0.1–0.2 µg m^{-3}	3160	7 %–30 %	0.01–0.02^b µg m^{-3}	–	–
PNC	270–1540 cm^{-3}	4262	3 %–16 %	27–154^b cm^{-3}	–	1 %–3 %
$PNC_{0.1}$ (UFP)	240–1390 cm^{-3}	4262	3 %–18 %	27–139^b cm^{-3}	–	1 %–3 %
PM_1 ($= PM_{2.5}$)	0.1–0.7 µg m^{-3}	4262	1 %–6 %	0.01–0.07^b µg m^{-3}	–	~ 1 %

[a] N_{peaks} is the total number of peaks the calculation was based on. [b] Values at RIV are estimated from values at BRI, assuming the same dilution factor than for CO_2.

with other studies (Keuken et al., 2014; Pohl et al., 2017). Peak heights of inland ships measured in direct proximity to the fairway were of similar magnitude to emissions from seagoing ships at a larger distance of about 200–800 m (Pirjola et al., 2014).

3.2 Additional contribution from shipping

The additional contribution from inland shipping to local background concentrations (composed of emissions from road traffic, industry, agriculture and residential heating) was calculated for both measurement stations in Worms as described in the Methods section. For each analyte a non-negligible background was reliably quantified and subtracted from significantly higher ship peaks, detected over a long period of time. The results are shown in Table 2 and, as explained in the Methods section, these values represent lower limits. We note that the additional contributions reported here were observed in close proximity to the shipping lane and were strongly dependent on meteorological conditions.

Monthly average concentrations of NO_x were increased by 6.9–14.3 µg m^{-3} at BRI (above the shipping lane) and by 1.0–2.2 µg m^{-3} at RIV (riverbank). This corresponds to an additional burden of 24 %–68 % and 6 %–11 %, respectively, relative to extrapolated background levels without the shipping contribution. The additional NO_2 load was 0.7–1.6 µg m^{-3} (3 %–10 %) at BRI and 0.3–0.5 µg m^{-3} (2 %–4 %) at RIV, whereby the higher dilution factor at RIV was partly compensated for by the increased NO to NO_2 conversion. Although a mean NO_2 contribution of a few percent can be considered relatively small, we note that it is strongly dependent on the meteorological conditions and can be substantially higher for a short period of time (e.g., up to 20 % on 16 April 2022 with wind from the eastern sector). In the case of RIV the derived values at a distance of 50–100 m to the shipping lane are in particular representative of the exposure of people staying here for an extended period of time. This includes walking, doing sports or having lunch, as well as company buildings and houses with gardens located close to the riverside. A comparable exposure can be expected on the riverbanks of other cities along the Rhine, albeit strongly

dependent on meteorological conditions and ship traffic density. Additional loads at BRI should be considered more of an upper limit for a maximum potential exposure. The increase in CO_2 due to shipping was ~ 0.1 % at BRI and ~ 0.01 % at RIV and thus negligible in terms of air quality (although relevant as a greenhouse gas contribution).

For BC the contribution at BRI was 0.1–0.2 µg m^{-3} corresponding to 7 %–30 %, whereas PM_1 was increased by 0.1–0.7 µg m^3 and 1 %–6 %. The increase of 3 %–16 % in PNC was dominated by small particles in the UFP range. Here our results underline the need for integrating UFP and BC measurements in air quality monitoring, as they are emitted by diesel engines in significant quantities and the fraction is highly relevant with respect to human exposure (WHO, 2021). Since particles were not measured at RIV with a sufficiently high temporal resolution to analyze the corresponding peaks (see Table 1), we estimated these values from the additional contribution derived at BRI by assuming the same dilution factor as for CO_2, i.e., a factor of ~ 10. Here we assumed that particle coagulation and chemical surface reactions were negligible due to the short atmospheric residence time of several seconds to a few minutes. This is in accordance with Kuittinen et al. (2021), who observed only marginal changes in the mean particle diameter over several minutes after emission. The background PNC required to calculate the relative contribution was taken from the (low-temporal-resolution) SMPS measurement.

3.3 Emission factors

Emission factors E_X (in g per kg fuel) were calculated for all measured components via Eqs. (1a)–(1c) (see Sect. 2.3.3). The analysis was performed for station BRI only to minimize uncertainties arising from the smaller sample size and the larger distance between ship and measurement inlet at RIV. Results are illustrated as box plots in Fig. 4 (for detailed statistics see Table S4).

We observed a large variability in emission factors for every component. This can be traced back to differing operating conditions and ship parameters, including high emitters as well as modern ships with exhaust gas aftertreatment,
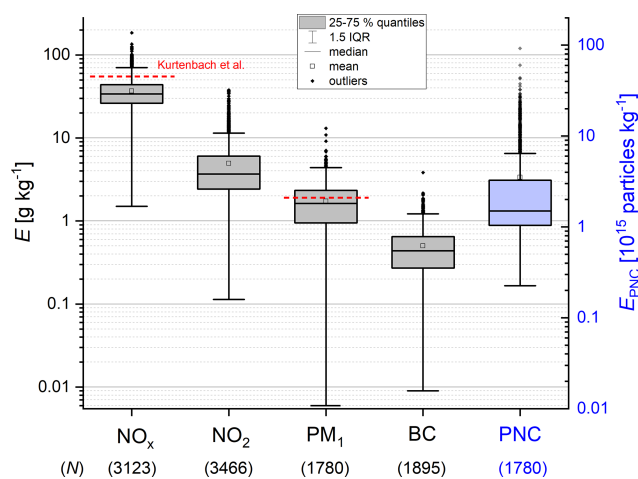
Figure 4. Boxplot of emission factors (E) measured at BRI and comparison with values reported by Kurtenbach et al. (2016) for the Lower Rhine in red. IQR signifies inter-quartile range. Numbers in parenthesis (N) indicate the sample size.

and will be discussed in Sect. 3.4 and 3.5. For NO_x a mean value of $E_{NO_x} = 37 \pm 16\,\mathrm{g\,kg^{-1}}$ was derived for the Upper Rhine section in Worms. This is significantly lower than the $52 \pm 3\,\mathrm{g\,kg^{-1}}$ reported by Kurtenbach et al. (2016) for the Lower Rhine between Wesel and Emmerich. For the Elbe River in Wedel a value of 40.9 ± 27.6 is reported by Kattner (2019), but here only inland ships with a length < 100 m were included in the analysis. The differences might be explained by different fleet characteristics and operating conditions. For further investigation we classified the ships by their length and width following the modified CEMT scheme suggested by Krause et al. (2023). For the most common ship classes observed in our study the differences in mean values were less than 15 % and the variability within single ship classes was high (see Table S5 for details) so that no clear trend could be derived. Compared with emission factors from the study of Krause et al. (2023) for the Lower Rhine close to Duisburg harbor (converted from $\mathrm{g\,s^{-1}}$ to $\mathrm{g\,kg^{-1}}$ using the fuel consumption scenario suggested by the authors), our values are on average 20 % to 40 % lower. This indicates potential differences in parameters like fleet composition, load status and operating conditions, as the ship traffic density on the Lower Rhine (Duisburg) is much higher than on the Upper Rhine (Worms) and as different goods are transported on different Rhine sections. These parameters can influence the mean emission factor, underlining the need for measurements at various locations. In general, NO_x emission factors derived for inland vessels are lower than the range of 53–68 $\mathrm{g\,kg^{-1}}$ observed for seagoing vessels (Diesch et al., 2013; Beecken et al., 2014; Kattner, 2019). However, considerably lower values can be observed for marine ships operating in emission control areas and vessels equipped with SCR technology (Sugrue et al., 2022). The NO_2 emission factor of

2.9 $\pm$ 2.5 $\mathrm{g\,kg^{-1}}$ (Fig. 4) at BRI was an order of magnitude lower than for NO_x, as during combustion most of the NO_x is emitted as NO. It has to be kept in mind that the emitted NO is rapidly converted to NO_2 so that the NO_2-to-NO_x ratio increases during plume transport. For this reason, NO_2 emission factors were not explicitly reported in other studies.

The emission factor for PNC was $E_{PNC} = (3.5 \pm 5.5) \times 10^{15}\,\mathrm{kg^{-1}}$ with the majority of particles situated in the UFP range (> 90 %). For the mass concentration we obtained $E_{PM} = 1.7 \pm 1.1\,\mathrm{g\,kg^{-1}}$ with about 30 % attributed to aerosol BC. For PM_1 a lower limit of 1.9 $\mathrm{g\,kg^{-1}}$ was reported by Kurtenbach et al. (2016), which is in line with our measurements, although their data were generated by an optical particle counter (OPC) detecting only particles above 0.25 μm diameter. According to our results they may underestimate the real-world PM emission factor. Further comparison with literature data is unfortunately impossible, as from the best of the authors' knowledge no other studies reporting PM or PNC emission factors for inland ships are available. For seagoing vessels E_{PM} values ranging from 2 to 3.3 $\mathrm{g\,kg^{-1}}$ are very similar to our results, whereas E_{PNC} was 2 to 7 times larger (Petzold et al., 2008; Jonsson et al., 2011; Lack and Corbett, 2012; Diesch et al., 2013; Beecken et al., 2014; Celik et al., 2020), probably due to the different fuel composition including the abovementioned higher sulfur content. The BC emission factor derived in this study ($E_{BC} = 0.5 \pm 0.3\,\mathrm{g\,kg^{-1}}$) is in the upper range of values reported for seagoing ships (Petzold et al., 2008; Diesch et al., 2013; Buffaloe et al., 2014; Jiang et al., 2018; Celik et al., 2020; Schlaerth et al., 2021; Sugrue et al., 2022), although there is a large variability in the literature depending on ship type, engine type, engine load, fuel and operating conditions.

3.3.1 Comparison with emission regulation limits

Calculated emission factors in grams per kilogram ($\mathrm{g\,kg^{-1}}$) were converted to energy-related values expressed in grams per kilowatt-hour ($\mathrm{g\,kWh^{-1}}$) following Eq. (4) and compared with existing emission regulations (see Table S1). This includes limits set by the Central Commission for the Navigation of the Rhine (CCNR, 2022) for newly registered motors since 2003 (CCNR I) and 2007 (CCNR II), as well as the Euro IIIa standard (which for the majority of inland ships is similar to CCNR II) and the recently introduced Euro V stage (2020), proposed by the EU (European Union, 2016). Here it is important to point out that these emission limits are based on test bench measurements under controlled laboratory conditions, whereas our results represent emission factors under real-world driving conditions for this particular Rhine section. Consequently, a limit exceedance cannot directly be concluded from our measurement data. Nevertheless, derived emission factors provide valuable insights, since vessels at the Rhine in Worms are operated under typical driving conditions and are thus a reasonable agreement should be achieved. For NO_x the resulting value of $(8.1 \pm 3.5)\,\mathrm{g\,kWh^{-1}}$

is approximately in line with emission limits for new motors since 2003 (CCNR I; see Table S1). For PM a mean emission factor of $(0.38 \pm 0.24)\,\text{g kWh}^{-1}$ was derived in our study, being slightly below CCNR I and above CCNR II standards. For PNC a limit of $1 \times 10^{12}\,\text{kWh}^{-1}$ was for the first time introduced with Euro V. Our calculated mean value of $(0.8 \pm 1.2) \times 10^{15}\,\text{kWh}^{-1}$ exceeds this limit by 3 orders of magnitude, but this is not surprising since up to now very few ships have been equipped with a new motor and such low values can only be achieved with the help of the DPF technology. A direct comparison for PM and PNC is difficult, anyway, as the emission limit refers to solid particles with diameters $> 23\,\text{nm}$, whereas our measurements include both the solid and the semi-volatile fraction of particles with diameters $> 6\,\text{nm}$. According to Petzold et al. (2008) and Giechaskiel et al. (2022) the semi-volatile fraction in exhaust emissions of diesel engines can be a substantial fraction in terms of PNC ($\sim 35\,\%$–$90\,\%$), whereby the contribution to PM is limited due to the small particle size. While the semi-volatile part is formed by ions and organics, the solid part is mostly elemental carbon, so the use of DPF does not necessarily result in a strong decrease in total PNC (Giechaskiel et al., 2022).

With the help of technical ship information data (see Sect. 2.2.3) we divided the observed ships into emission categories based on the limit the ship engines have to comply with (see Fig. 5 and Table S1). For vessels fulfilling the CCNR I standard we derived a value of $(8.9 \pm 3.2)\,\text{g kWh}^{-1}$ for NO$_x$ which agrees very well with the corresponding emission limit of $9.2\,\text{g kWh}^{-1}$. Analysis of CCNR II vessels resulted in a mean emission factor of $(8.7 \pm 3.2)\,\text{g kWh}^{-1}$, which is slightly above the limit of $6\,\text{g kWh}^{-1}$. For Euro IIIa vessels with a mean emission factor of $(7.0 \pm 2.5)\,\text{g kWh}^{-1}$ a better agreement is achieved. For Euro V vessels the measured emission factor of $(0.6 \pm 0.5)\,\text{g kWh}^{-1}$ is a factor of 3 below the limit, although based on very few data points, as we captured only three ships equipped with such a modern engine. This low value and the $\sim 90\,\%$ NO$_x$ reduction compared to CCNR II vessels agree very well with observations made by CLINSH (2022). With regard to PM emission factors, CCNR I vessels are well below the limit (Fig. 5), whereas for CCNR II and Euro IIIa vessels the corresponding limit is exceeded by a factor of 2 on average. This could indicate that real-world particle emissions might not be as efficiently reduced as under test bench conditions. Potential reasons for this are malfunctions and unfavorable operating conditions, e.g., a low engine load (Gysel et al., 2016; Sugrue et al., 2022). However, we have to keep in mind the relatively large uncertainty arising from the estimate for the particle density (Sect. 2.2.2) and the substantial fraction of measured semi-volatile particles discussed above. The number of measurements for Euro V vessels was very limited, but results suggest that requirements were fulfilled through the application of DPF. This is in line with a $\sim 90\,\%$ PM reduction ob-
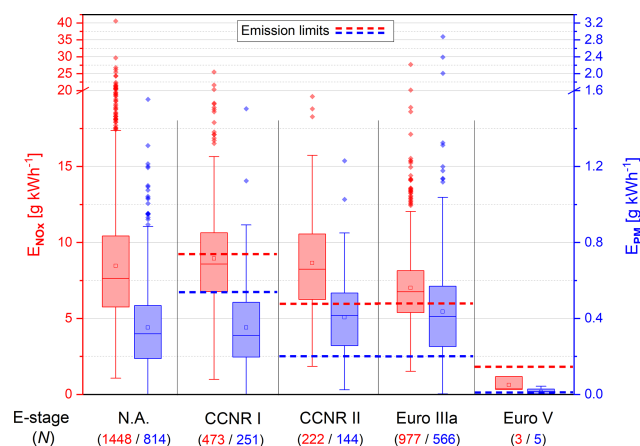

Figure 5. Comparison of NO$_x$ and PM emission factors (E) from this study with existing limits (dashed red line for NO$_x$, blue for PM) per emission stage category (see Table S1): CCNR I standard (valid from 2003 on), CCNR II (2007), Euro IIIa (2007) and Euro V (2020). Boxplot: box signifies $25\,\%$ to $75\,\%$ quantiles, whisker signifies IQR, square signifies mean, and solid line signifies median. The numbers in parentheses indicate the number of NO$_x$ and PM peaks the box plot is based on. N.A. means information is not available from the ship database.

served in the literature for DPF technology applied in marine engines (Gysel et al., 2016).

We also detected a small number of ships ($\sim 5\,\%$) where the plume was characterized by very low BC levels (often below the detection limit), sometimes in combination with an extraordinary high NO$_2$-to-NO$_x$ ratio (up to $50\,\%$). This indicates the use of aftertreatment systems with catalyst and DPF, where high NO$_2$ levels in the exhaust are favored for the filter regeneration. Unfortunately, we do not have any information about potential filtering technology used on board (only about the engine itself).

Overall, our dataset underlines the large emission reduction potential when modernizing the engines of inland vessels. In this study $\sim 30\,\%$ of the fleet's motors were fulfilling the Euro IIIa standard and only $\sim 0.1\,\%$ the recent Euro V standard. Assuming a future scenario where $50\,\%$ of the ships have been equipped with a Euro IIIa stage motor and $50\,\%$ with a Euro V motor would already halve the NO$_x$ and PM emissions based on our collected data. A complete transition to the Euro V standard would even reduce NO$_x$ and PM emissions by more than $90\,\%$. In particular, the use of DPF technology would also result in a drastic reduction in BC. Referring to Table 2, the additional NO$_2$ contribution from shipping at BRI and RIV could be reduced to $0.12\,\mu\text{g m}^{-3}$ and $0.04\,\mu\text{g m}^{-3}$, respectively, corresponding to less than $1\,\%$ of the total NO$_2$ emissions. Similarly, the PM contribution from shipping could be reduced to $0.04\,\mu\text{g m}^{-3}$ ($0.5\,\%$) at BRI directly above the shipping lane. An accelerated modernization of the fleet would thus have a measurable impact on local air quality, especially when transferring the obser-
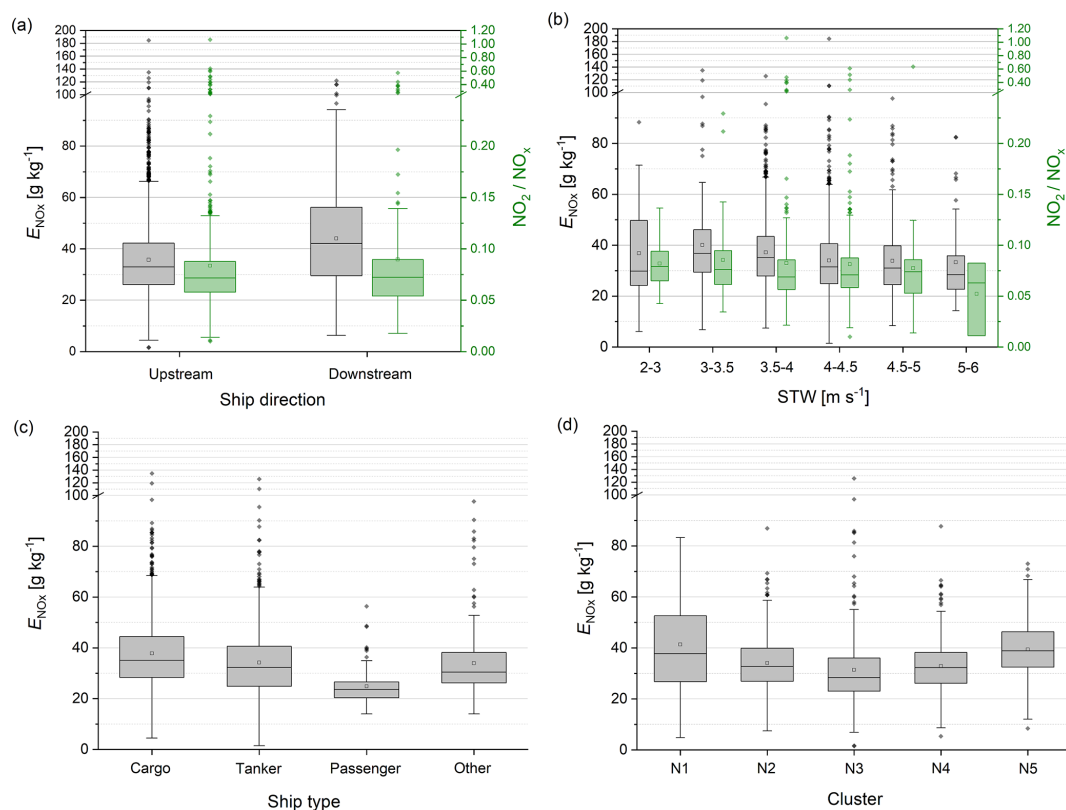
Figure 6. Influence of ship parameters on NO_x emission factor (E_{NO_x}) and NO_2-to-NO_x ratio: **(a)** traveling direction, **(b)** speed through water (STW), **(c)** ship type and **(d)** clusters based on engine characteristics (see Table 3). For better readability the scaling of the y axis was adapted for $E_{NO_x} > 100\,\mathrm{g\,kg^{-1}}$ and $NO_2/NO_x > 0.25$.

vations to more heavily frequented sections along the Lower Rhine (e.g., Duisburg).

3.4 Dependence of NO_x emissions on ship parameters

The large variability in NO_x emission factors (E_{NO_x}) observed in this study is consistent with other field studies dealing with inland shipping (Kurtenbach et al., 2016; Krause et al., 2023) and raises the question of potential influencing factors. In the following the effects of operating conditions (direction of travel, speed through water) and ship parameters (ship type, engine characteristics) on emissions are brought into context. Generally speaking, the dependence of emissions on ship parameters and atmospheric conditions is very complex and variable from ship to ship. For inland ships there is little information available in the literature, whereas for seagoing ships detailed studies or reviews are, e.g., provided by Buffaloe et al. (2014), Celik et al. (2020), Grigoriadis et al. (2021), and Sugrue et al. (2022).

At the Rhine in Worms we observed a decrease in E_{NO_x} at higher engine loads, i.e., for upstream ships compared to downstream ships (Fig. 6a). In contrast, the NO_2-to-NO_x ratio was very similar, indicating no significant differences in plume age. With regard to the vessel speed (Fig. 6b) we no-

ticed a slightly decreasing E_{NO_x} with increasing STW (except for very low speeds). A high steady-state engine load is commonly related to a higher combustion temperature and a more complete combustion process, resulting in a positive correlation between STW and engine load and E_{NO_x}, especially for seagoing ships with high-powered motors (Cappa et al., 2014; Celik et al., 2020). On the other hand, a higher engine load can lead to a reduction in the air-to-fuel ratio and thus in the oxygen content, resulting in reduced NO_x formation, which is assumed to have a major effect for inland ship engines in this study. Simultaneously, the NO_2-to-NO_x ratio tends to decrease with increasing STW (Fig. 6b). This can be traced back to the higher combustion temperatures leading to enhanced NO formation and is in line with observations for seagoing ships (Celik et al., 2020). For inland ships, the generally weak dependence of emission factors on engine load under normal operating conditions observed in this study is in line with the observations of Kurtenbach et al. (2016) and CLINSH (2022) and suggests the existence of other influencing parameters.

In addition to dynamic operating conditions, inland vessels were distinguished by their type, whereby cargo, tanker and passenger ships are of major significance on the Upper Rhine. Figure 6c shows that, with an average of $33\,\mathrm{g\,kg^{-1}}$,

Table 3. Overview of clusters based on engine characteristics and ship dimensions together with average NO_x emission factors (E_{NO_x}).

Cluster	Motor age[a]	Power[b] (kW)	rpm[c]	Ship length[d]	Ship width[e]	E_{NO_x} (g kg^{-1})	NO_2/NO_x	N_{peaks}
N1	Old	Low	Low	Low	Low	41.4 ± 18.2	0.06 ± 0.03	92
N2	Medium	Medium	High	High	High	34.1 ± 11.5	0.10 ± 0.10	244
N3	Medium	Low	High	Medium	Medium	31.4 ± 13.4	0.08 ± 0.05	350
N4	Medium	High	High	Medium	Medium	32.8 ± 9.8	0.08 ± 0.03	450
N5	Medium	High	Medium	Medium	Medium	39.4 ± 11.9	0.07 ± 0.04	145

[a] Motor age (mean): old (1970–1972), medium (2011–2013). [b] Power (mean): low (670–720), medium (1090–1110), high (1170–1200).
[c] Revolutions per minute (rpm) of motor (mean): low (550–570), medium (940–970), high (1600–1780). [d] Ship length (mean): small
(90–95), medium (105–125), large (170–175). [e] Ship width (mean): small (9–10), medium (11–12), large (14).
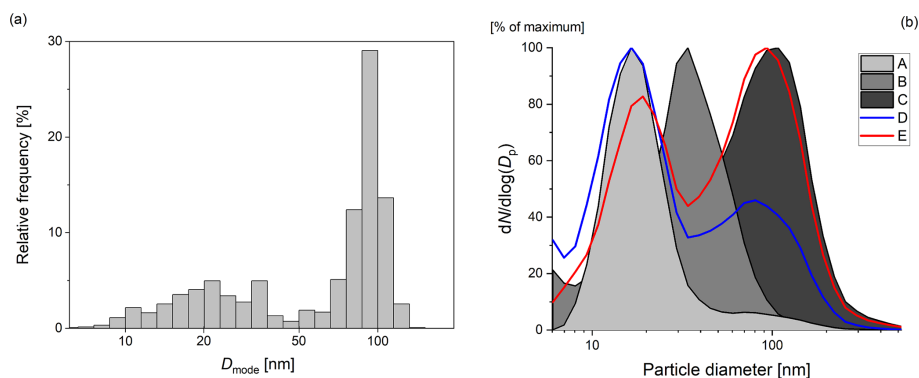
Figure 7. (a) Relative abundance of the particle mode diameter (D_{mode}) for upstream ships based on 1503 peaks. **(b)** Exemplary particle size distribution (PSD) from five ships (labeled A–E).

cargo ships had the highest mean NO_x emission factor, while it was 10 % lower for tankers and 35 % lower for passenger ships. A possible explanation is a more frequent modernization for the latter type of ships. This finding is consistent with Pirjola et al. (2014) and Kattner (2019), and a similar tendency was observed for seagoing ships in the Baltic and North Sea (Beecken et al., 2014). Excluding passenger ships, the influence of ship type and operating conditions on the E_{NO_x} can be considered rather small and is not sufficient to explain the observed variability in our dataset.

As a consequence, we investigated the effect of engine characteristics like motor power or revolutions per minute (rpm) by performing a cluster analysis (see Sect. 2.3.4), with the five clusters based on 1281 ship peaks described in Table 3. The effect on NO_x emission factors is illustrated in Fig. 6d and reveals that for cluster N1, containing ships equipped with old motors (mean year of construction 1972), low power (< 700 kW) and low rpm (< 600), NO_x emission factors were enhanced by 20 % to 30 % compared to clusters N2, N3 and N4. Increased NO_x emission factors were also observed for medium-aged motors with high power but medium rpm (cluster N5). This is consistent with the positive correlation between power and NO_x emissions found for seagoing ships (Diesch et al., 2013). In contrast, low emissions were observed for relatively new motors with high rpm

(clusters N2–N4), closest to the motor type used in modern trucks. Our findings are consistent with literature studies for seagoing ships in which motors with high power and low rpm are associated with larger emissions compared to motors with low power and high rpm (Grigoriadis et al., 2021). This is mainly due to a longer residence time in the combustion chamber at low rpm, leading to an enhanced NO_x content in the exhaust gas (Reif, 2012).

3.5 Dependence of particle emissions on ship parameters

The mean particle size distribution (PSD) from 6 to 520 nm based on 1822 ship peaks showed a unimodal size distribution for up- and downstream vessels with a geometric mean particle diameter of 52 ± 23 nm and a mode diameter (D_{mode}) of 66 ± 35 nm. On average, the majority of particles was found in the Aitken mode, which is consistent with results from Pohl et al. (2017) for inland vessels on the Lower Rhine. Figure 7a describes the relative abundance of the mode diameter (D_{mode}), i.e., the channel where the highest particle count was measured. This distribution has a bimodal appearance, although each ship's individual peak was normally characterized by a unimodal size distribution with the mode diameter being highly variable from ship to ship (Fig. 7b, A–

C). For both traveling directions there are ships which emit the majority of particles in the range of 10–40 nm (nucleation mode) and ships where this maximum lies in the range of 60–110 nm (Aitken mode). For a small number of ship plumes both modes also existed at the same time with either the nucleation (Fig. 7b, D) or the Aitken mode (Fig. 7b, E) being dominant. For diesel engines bimodal distributions are typical, but it depends on various parameters which mode exists or dominates (Kittelson, 1998). Particles in the nucleation mode are mostly hydrocarbons from lubrication oil, unburnt fuel, water vapor or sulfur particles. Old inland ship engines and engines with low rpm (two-stroke diesel) typically show a pronounced nucleation peak. The accumulation mode consists mainly of ash (elemental carbon, EC) and is a typical feature of diesel car engines. In this regard it is important to mention that the actual size distribution can be highly individual depending on the engine and the DPF used.

A comparison of inland ships with oceangoing vessels is only reasonable to a limited extent, as the larger sulfur content affects the total number of particles and results in a pronounced nucleation mode (Celik et al., 2020; Diesch et al., 2013; Pirjola et al., 2014; Zhou et al., 2019). This is due to the conversion of SO_2 to SO_3 in the catalyst and reaction with water molecules forming gaseous sulfuric acid (Karjalainen et al., 2014). The D_{mode} of ships with low sulfur content is usually between 30 and 60 nm, which is similar to our study. With higher sulfur content, the particles become slightly larger (Zhou et al., 2019). Significant increases in PNC at a diameter > 250 nm were not measured in other studies (Diesch et al., 2013; Beecken et al., 2015; Ausmeel et al., 2019; Kuittinen et al., 2021); i.e., particles are exclusively detected in the UFP range, consistent with emissions from inland vessels in this study. Depending on ship characteristics both uni- and bimodal size distributions were observed by others (Jonsson et al., 2011; Diesch et al., 2013; Pirjola et al., 2014; Beecken et al., 2015). Furthermore, when comparing inland and seagoing vessels, a higher relative speed or a higher engine load leads to higher emissions for inland vessels, while the opposite is the case for seagoing diesel engines. Here, cleaner combustion takes place when the ships are operated under high load, resulting in lower emissions (Pohl et al., 2017).

A more reasonable comparison is possible with diesel-powered road transport due to the same fuel. Several studies show a predominance of UFP (Chatain et al., 2021; Kwasny et al., 2010), similar to emissions from inland shipping in this study. The main difference is the use of catalysts and particulate filters in road transport which are rarely applied in inland ships so far. This alters the PSD and PNC in the exhaust gas and results in a varying manifestation of nucleation and accumulation mode. Older cars without particulate filter and partly with sulfur-containing diesel cause a bimodal peak (Giechaskiel et al., 2005). For newer vehicles with particulate filters, a reduction in particulates in the nucleation

mode was observed, resulting in a unimodal PSD (Braisher et al., 2010; Li et al., 2018).

In this study PNC, PM and also PSD were influenced by different ship-related parameters. In the following, the impact of STW, ship type, engine power, revolutions per minute (rpm) and year of construction was analyzed. Figure 8a shows that the PNC emission factor (E_{PNC}) for downstream ships is higher than for upstream ships. At the same time particles of downstream ships have a slightly smaller mode diameter (D_{mode}) and geometric mean diameter (GMD) than upstream ships. This may result from differences in the fuel consumption. Ships tend to use more fuel when traveling upstream, which means increased particle generation and more particles per volume in the exhaust pipe and thus in the plume. In a high-density plume, nucleation-mode particles can coagulate faster on the way from the exhaust to the point of measurement, resulting in an increased mean particle diameter. With a BC fraction (relative to total PM) of 38 % for upstream ships and 16 % for downstream ships our results indicate that a higher engine load leads to an increase in BC emission. This is in line with studies by Jiang et al. (2018) and Schlaerth et al. (2021) on smaller marine engines (like passenger ships and tugboats) but is in contrast to Buffaloe et al. (2014) and Celik et al. (2020), who measured a decrease in BC with increasing engine load. The large variability in BC emission factors reported in the literature reflects the influence of engine type, fuel type and operating conditions. From multi-wavelength analysis of the AE33 (Sandradewi et al., 2008) we derived a mean fractional contribution from biomass burning of ~ 10 %, indicative of organic aerosol components that might be formed during the combustion of ship diesel blended with biofuel.

No clear correlation between STW and D_{mode} was found (Fig. 8b). The highest E_{PNC} was observed for ships with a speed of 2–3 and 5–6 m s^{-1}; i.e., exceptionally low or high engine loads tend to result in higher emission factors. These groups also contained the lowest mean D_{mode} with 47 nm for 2–3 m s^{-1} and 56 nm for 5–6 m s^{-1}. The classification into ship types showed the highest mean E_{PNC} for passenger ships (and thus the opposite trend than for NO_x; see above), whereas D_{mode} (and E_{BC}; see Supplement) was the lowest (Fig. 8c).

For a classification based on ship size, ships were often divided into ship classes in past studies (Kurtenbach et al., 2016; Krause et al., 2023). This division showed that smaller ships were tendentially characterized by larger E_{PNC} and lower D_{mode} (see Table S5). But small ships are usually older and have lower engine power and rpm. Thus, it is probably not the length and width of the ships included in the ship classes that are decisive for D_{mode} and E_{PNC} but the engine. Based on these findings, a cluster analysis using particle data from upstream vessels (683 peaks from 341 ships) and corresponding engine data was done (see Sect. 2.3.4). Figure 8d shows the frequency distribution of D_{mode} and E_{PNC} for each cluster. Cluster P2 was characterized by old engines with a
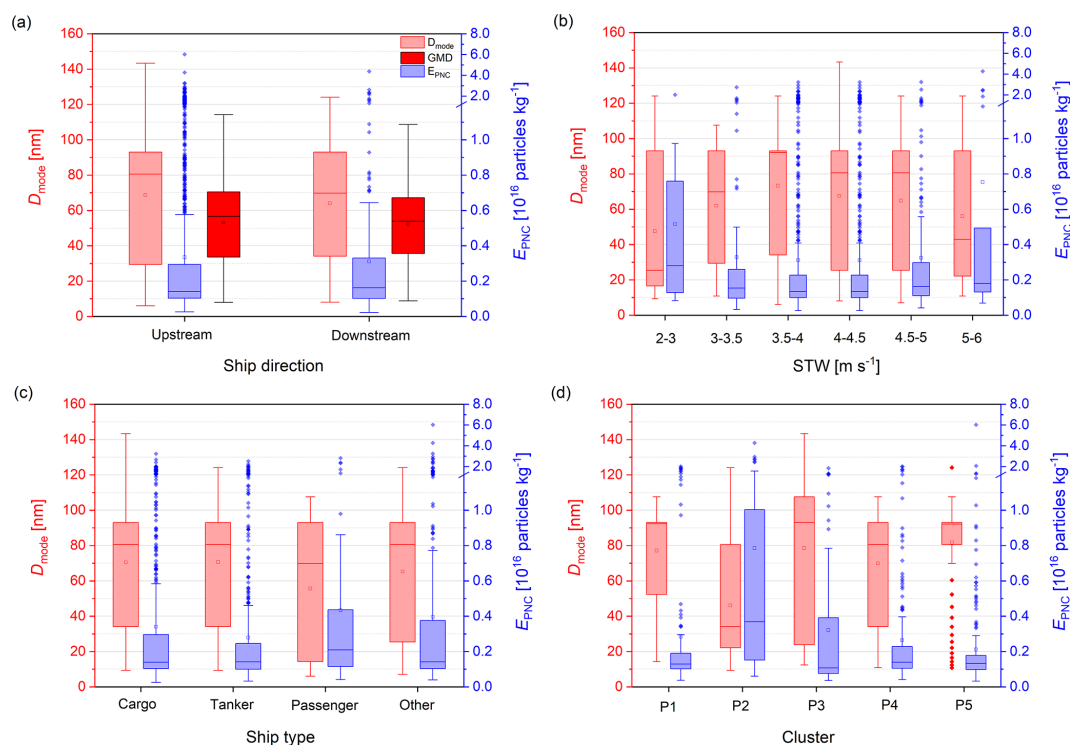
Figure 8. Influence of ship parameters on PNC emission factor (E_{PNC}) and particle mode diameter (D_{mode}): **(a)** traveling direction, **(b)** speed through water (STW), **(c)** ship type and **(d)** clusters based on engine characteristics (see Table 4). For better readability the scaling of the y axis was adapted for $E_{PNC} > 1.2 \times 10^{16}\,\mathrm{kg}^{-1}$.

Table 4. Overview of clusters based on engine characteristics and ship dimensions together with average PNC emission factors (E_{PNC}).

Cluster	Motor age[a]	Power[b] (kW)	rpm[c]	Ship length[d]	Ship width[e]	E_{PNC} (kg^{-1})	D_{mode} (nm)	N_{peaks}
P1	Medium	Medium	High	High	High	$(2.8 \pm 4.3) \times 10^{15}$	77 ± 32	126
P2	Old	Low	Low	Low	Low	$(7.8 \pm 9.5) \times 10^{15}$	46 ± 30	46
P3	Medium	High	Medium	Medium	Medium	$(3.2 \pm 4.3) \times 10^{15}$	79 ± 42	60
P4	Medium	Low	High	Medium	Medium	$(2.6 \pm 3.4) \times 10^{15}$	70 ± 31	177
P5	Medium	High	High	Medium	Medium	$(2.1 \pm 4.1) \times 10^{15}$	82 ± 28	274

[a] Motor age (mean): old (1970–1972), medium (2011–2013). [b] Power (mean): low (670–720), medium (1090–1110), high (1170–1200).
[c] Revolutions per minute (rpm) of motor (mean): low (550–570), medium (940–970), high (1600–1780). [d] Ship length (mean): small (90–95), medium (105–125), large (170–175). [e] Ship width (mean): small (9–10), medium (11–12), large (14).

mean year of construction of 1970, low rpm, low power, and small width and length (Table 4). It shows the smallest particles with a mean D_{mode} of 46 nm. Also, E_{PNC} was highest for this cluster with $7.8 \times 10^{15}\,\mathrm{kg}^{-1}$. This means that data from engines with an older age with low power and low rpm were characterized by high E_{PNC} and comparably small particles. For cluster P5, which reflects ships with modern engines, $E_{PNC} = 2.1 \times 10^{15}\,\mathrm{g\,kg}^{-1}$ is low compared to the other clusters and the D_{mode} mean of 82 nm is also highest. This could be due to a more complete combustion by the newer engine and thus a less developed nucleation mode. Thus, it can be concluded that the different PSD and PNC result from

different engine characteristics, in particular the motor age, power and rpm.

Unfortunately, there are no other studies explicitly addressing the impact of engine characteristics of inland ships on particle emissions. Studies of inland ship emissions related to PM show a positive correlation with power or speed (Busch et al., 2020). However, analyzed vessels at berth show a negative correlation with power but a positive one with age (Busch et al., 2021). In our study, no influence of these parameters on PM was evident. For seagoing ships an increase in PNC for diameters > 100 nm is associated with decreasing speed and attributed to incomplete combustion (Diesch et al.,

2013). Other factors influencing the PSD were, similar to our results, the year of construction and the power (Diesch et al., 2013; Pirjola et al., 2014). The differences between the individual clusters for both particles and NO_x (see Sect. 3.4) suggest that motor age, rpm and engine power have the largest effect on the emission factor of inland ships, while ship size and STW only play a minor role under normal operating conditions.

4 Conclusions

We investigated the contribution of inland shipping to air pollution based on emission measurements for the river Rhine in Worms, Germany. Measurements were carried out over the course of more than 1 year at two measurement stations in direct vicinity to the Rhine (one directly above the lane, one on the riverbanks) and represent the first long-term on-shore measurements available for the Upper Rhine. By combining a peak analysis algorithm with AIS data, the monthly average contribution from inland shipping (NO_x, NO_2, PNC, UFP, PM_1 and BC) was derived for the two measurement stations and put into relation to atmospheric background levels. For NO_2 a monthly mean contribution of 7 % in addition to the local background concentration was calculated for BRI and 3 % for RIV. Directly above the shipping lane at BRI shipping led to an increase of 50 % in NO_x, whereas PNC was increased by 10 %, PM_1 by 4 % and BC by 15 %. The majority of particles was measured in the UFP range ($\sim$ 75 %), with a dominance of the Aitken mode. The contribution from shipping was highly variable from day to day, depending on prevailing wind conditions. Although not being representative of other parts of the city of Worms, our measurements provide a useful estimate of the typical exposure of people living or working very close to the Rhine.

The applied peak analysis mechanism can easily be transferred to other locations as long as CO_2 and AIS data are collected together with the compound of interest (e.g., NO_x or PM). Prerequisites facilitating the analysis are that the station is close to the river (peaks distinguishable from noise), the traffic density is not too high (no peak overlap), and the variability in the background signal (arising from non-ship emission sources like road traffic) is low on timescales of minutes. The advantage of our method is that is does not rely on dispersion modeling and that energy-related emission factors are transferable to other locations, fleets and operating conditions (although the fuel consumption has to be carefully estimated). This enables its application in emission inventories and modeling studies to more accurately calculate the exposure of people to air pollution along inland waterways.

The observed PSD of inland ships and the large proportion of UFP highlight the necessity to integrate UFP measurements in future studies, especially with regard to the recommendations for action of the WHO, where a more in-depth research of UFP is requested (WHO, 2021). In particular optical measuring devices that are not able to detect particles < 100 nm are not suitable to be applied in the specific case of shipping emissions and may bias the results when operated alone. This study also underlines the necessity of considering inland vessels separately, since results from studies about seagoing ships or road transport cannot easily be transferred due to differences in motor dimensions, driving conditions, fuel sulfur content and particle filtering technology, although the dominance of UFP is a common feature.

From single ship plumes we derived realistic emission factors for the fleet on the Upper Rhine in Worms under real-driving conditions, complementing existing studies at the Lower Rhine. Reported NO_x emission factors were on average lower than at the Lower Rhine and approximately in line with requirements set by the CCNR and the EU, whereas PM emission factors were slightly increased. This might be due to a decreased emission reduction efficiency in real-world operations compared with test bench conditions. For the small number of ships with modern Euro V diesel engines and aftertreatment systems passing the station, we derived very low NO_x and PM emission factors, underlining their emission reduction potential. Increasing the percentage of motors fulfilling the Euro IIIa and the Euro V standards to 50 % each would already halve emissions in close vicinity to the shipping lane. A complete transition to Euro V has the potential to reduce them by $\sim$ 90 % and to improve air quality in cities along inland rivers with heavier ship traffic and port activities than observed for Worms. A detailed analysis with respect to ship direction, STW, ship type and ship class revealed that the large observed variability in emission factors could hardly be accessed by classification schemes commonly used in the literature. Using additional technical data about the ship engines, we figured out that both gaseous and particulate emissions were strongly dependent on engine characteristics (especially rpm and power). Particularly, old ships with low rpm and power caused high emission factors for both NO_x and PNC, whereby the PSD was characterized by a small particle mode diameter. These findings underline the need to overcome limitations in data accessibility, as the use of emission factors related to engine-specific data (which are not automatically sent via AIS) can help to improve impact calculations of inland shipping in modeling studies. In addition, the results illustrate the potential of long-term on-shore measurements to monitor future effects of fleet modernization, i.e., emission reduction by replacing or retrofitting engines with DPF or exhaust gas aftertreatment systems.

For future studies we aim to additionally measure particle composition (e.g., via aerosol mass spectrometry, AMS) to derive a realistic estimate for the particle density. The existing databases could also be extended by further measurements at different Rhine sections and along other relevant waterways in Europe in order to capture various fleet compositions and driving conditions. For a more detailed investigation of the plume dispersion in cities along rivers a monitor-

ing network with sensors placed at different distances to the shipping lane in combination with measurements on board and a small-scale modeling approach would be of significant value.

Author contributions. TM and PE wrote the manuscript with contributions from AZ and LD. Measurements in Worms were conducted by TM and PE with AZ supporting the setup of the measurement equipment. TM and PE performed the data analysis with TM focusing on particles and the influence of ship and engine parameters on emissions and PE focusing on NO$_x$, the peak detection algorithm and the derivation of emission factors.

References

Alföldy, B., Lööv, J. B., Lagler, F., Mellqvist, J., Berg, N., Beecken, J., Weststrate, H., Duyzer, J., Bencs, L., Horemans, B., Cavalli, F., Putaud, J. P., Janssens-Maenhout, G., Csordás, A. P., Van Grieken, R., Borowiak, A., and Hjorth, J.: Measurements of air pollution emission factors for marine transportation in SECA, Atmos. Meas. Tech., 6, 1777–1791, https://doi.org/10.5194/amt-6-1777-2013, 2013.

Ausmeel, S., Eriksson, A., Ahlberg, E., and Kristensson, A.: Methods for identifying aged ship plumes and estimating contribution to aerosol exposure downwind of shipping lanes, Atmos. Meas. Tech., 12, 4479–4493, https://doi.org/10.5194/amt-12-4479-2019, 2019.

Barone, T. L., Lall, A. A., Storey, J. M. E., Mulholland, G. W., Prikhodko, V. Y., Frankland, J. H., Parks, J. E., and Zachariah, M. R.: Size-Resolved Density Measurements of Particle Emissions from an Advanced Combustion Diesel Engine: Effect of Aggregate Morphology, Energy Fuels, 25, 1978–1988, https://doi.org/10.1021/ef200084k, 2011.

Beecken, J., Mellqvist, J., Salo, K., Ekholm, J., and Jalkanen, J. P.: Airborne emission measurements of SO$_2$, NO$_x$ and particles from individual ships using a sniffer technique, Atmos. Meas. Tech., 7, 1957–1968, https://doi.org/10.5194/amt-7-1957-2014, 2014.

Beecken, J., Mellqvist, J., Salo, K., Ekholm, J., Jalkanen, J. P., Johansson, L., Litvinenko, V., Volodin, K., and Frank-Kamenetsky, D. A.: Emission factors of SO$_2$, NO$_x$ and particles from ships in Neva Bay from ground-based and helicopter-borne measurements and AIS-based modeling, Atmos. Chem. Phys., 15, 5229–5241, https://doi.org/10.5194/acp-15-5229-2015, 2015.

Birks, J. W., Andersen, P. C., Williford, C. J., Turnipseed, A. A., Strunk, S. E., Ennis, C. A., and Mattson, E.: Folded tubular photometer for atmospheric measurements of NO$_2$ and NO, Atmos. Meas. Tech., 11, 2821–2835, https://doi.org/10.5194/amt-11-2821-2018, 2018.

Braisher, M., Stone, R., and Price, P.: Particle number emissions from a range of European vehicles, SAE Technical Paper 0148-7191, SAE, https://doi.org/10.4271/2010-01-0786, 2010.

Buffaloe, G. M., Lack, D. A., Williams, E. J., Coffman, D., Hayden, K. L., Lerner, B. M., Li, S. M., Nuaaman, I., Massoli, P., Onasch, T. B., Quinn, P. K., and Cappa, C. D.: Black carbon emissions from in-use ships: a California regional assessment, Atmos. Chem. Phys., 14, 1881–1896, https://doi.org/10.5194/acp-14-1881-2014, 2014.

Busch, D., Brandt, A., Kleinebrahm, M., and Dreger, S.: Emission measurements on the laboratory vessel "Max Prüss" after retrofitting with a SCRT system, Clean Inland Shipping (CLINSH) Landesamt für Natur Umwelt und Verbraucherschutz Nordrhein-Westfalen (LANUV), Recklinghausen, https://www.clinsh.eu/controllers/download.php?filename=7_Max_Pruss_report/Max_Pr%C3%BCss_report_English.pdf (last access: 7 August 2023), 2020.

Busch, D., Bergen, A., Hoogma, R., and Lubbering, E.: CLINSH Deliverable: B.4 Modelling, evaluating and scenario building: Harbour monitoring Part B: Determination of NO$_x$ and particulate matter emissions from inland vessels at berth, Landesamt für Natur, Umwelt und Verbraucherschutz (LANUV) Nordrhein-Westfalen, Recklinghausen, https://www.clinsh.eu/controllers/

download.php?filename=8_Harbour_monitoring/part_B.pdf (last access: 7 August 2023), 2021.

Cao, Y. L., Wang, X., Yin, C. Q., Xu, W. W., Shi, W., Qian, G. R., and Xun, Z. M.: Inland Vessels Emission Inventory and the emission characteristics of the Beijing-Hangzhou Grand Canal in Jiangsu province, Proc. Safe. Environ. Protect., 113, 498–506, https://doi.org/10.1016/j.psep.2017.10.020, 2018.

Cappa, C. D., Williams, E. J., Lack, D. A., Buffaloe, G. M., Coffman, D., Hayden, K. L., Herndon, S. C., Lerner, B. M., Li, S. M., Massoli, P., McLaren, R., Nuaaman, I., Onasch, T. B., and Quinn, P. K.: A case study into the measurement of ship emissions from plume intercepts of the NOAA ship Miller Freeman, Atmos. Chem. Phys., 14, 1337–1352, https://doi.org/10.5194/acp-14-1337-2014, 2014.

CCNR: Central Commission for the Navigation of the Rhine, Annual report 2018, Inland navigation in Europe, Market Observation, https://www.ccr-zkr.org/files/documents/om/om18_II_en.pdf (last access: 7 August 2023), 2018.

CCNR: Central Commission for the Navigation of the Rhine, Annual Report, Inland Navigation in Europe, Market Observation, https://www.ccr-zkr.org/files/documents/om/om21_II_en.pdf (last access: 7 August 2023), 2021.

CCNR: Central Commission for the Navigation of the Rhine, CCNR Roadmap for reducing inland navigation emissions, https://www.ccr-zkr.org/files/documents/Roadmap/Roadmap_en.pdf (last access: 7 August 2023), 2022.

Celik, S., Drewnick, F., Fachinger, F., Brooks, J., Darbyshire, E., Coe, H., Paris, J. D., Eger, P. G., Schuladen, J., Tadic, I., Friedrich, N., Dienhart, D., Hottmann, B., Fischer, H., Crowley, J. N., Harder, H., and Borrmann, S.: Influence of vessel characteristics and atmospheric processes on the gas and particle phase of ship emission plumes: in situ measurements in the Mediterranean Sea and around the Arabian Peninsula, Atmos. Chem. Phys., 20, 4713–4734, https://doi.org/10.5194/acp-20-4713-2020, 2020.

CEMT – European Conference of Ministers of Transport: Resolution No. 92/2 on new classification of inland waterways (CEMT/CM(92)6/FINAL), https://www.itf-oecd.org/resolution-no-922-new-classification-inland-waterways (last access: 7 August 2023), 1992.

Chatain, M., Alvarez, R., Ustache, A., Riviere, E., Favez, O., and Pallares, C.: Simultaneous Roadside and Urban Background Measurements of Submicron Aerosol Number Concentration and Size Distribution (in the Range 20–800 nm), along with Chemical Composition in Strasbourg, France, Atmosphere, 12, 71, https://doi.org/10.3390/atmos12010071, 2021.

CLINSH: Clean Inland Shipping (CLINSH) – Deliverable B3.2, Develop NO_x emission factors through data from CLINSH measurements, https://www.clinsh.eu/iu-assets/4/3_CLINSH_NOx_emission_factors.pdf (last access: 7 August 2023), 2022.

Cooper, D. A.: Exhaust emissions from high speed passenger ferries, Atmos. Environ., 35, 4189–4200, https://doi.org/10.1016/S1352-2310(01)00192-3, 2001.

Diesch, J. M., Drewnick, F., Klimach, T., and Borrmann, S.: Investigation of gaseous and particulate emissions from various marine vessel types measured on the banks of the Elbe in Northern Germany, Atmos. Chem. Phys., 13, 3603–3618, https://doi.org/10.5194/acp-13-3603-2013, 2013.

Drinovec, L., Mocnik, G., Zotter, P., Prevot, A. S. H., Ruckstuhl, C., Coz, E., Rupakheti, M., Sciare, J., Muller, T., Wiedensohler, A., and Hansen, A. D. A.: The "dual-spot" Aethalometer: an improved measurement of aerosol black carbon with real-time loading compensation, Atmos. Meas. Tech., 8, 1965–1979, https://doi.org/10.5194/amt-8-1965-2015, 2015.

Eger, P., Mathes, T., Zavarsky, A., and Duester, L.: Dataset for 'Inland ship emissions and their contribution to NO_x and ultrafine particle concentrations at the Rhine', Zenodo [data set], https://doi.org/10.5281/zenodo.7896435, 2023.

European Comission: NAIADES III action plan, https://eur-lex.europa.eu/legal-content/EN/TXT/?uri=CELEX:52021DC0324 (last access: 7 August 2023), 2021.

European Union: Richtlinie 2008/50/EG des Europäischen Parlaments und des Rates vom 21. Mai 2008 über Luftqualität und saubere Luft für Europa, 1–44, https://eur-lex.europa.eu/eli/dir/2008/50/oj (last access: 7 August 2023), 2008.

European Union: Regualtion (EU) 2016/1628 of the european parliament and of the council of 14 September 2016 on requirements relating to gaseous and particulate pollutant emission limits and type-approval for internal combustion engines for non-road mobile machinery, amending Regulations (EU), No. 1024/2012 and (EU) No. 167/2013, and amending and repealing Directive 97/68/EC, Official Journal of the European Union, https://eur-lex.europa.eu/eli/reg/2016/1628/oj (last access: 7 August 2023), 2016.

Eyring, V., Isaksen, I. S. A., Berntsen, T., Collins, W. J., Corbett, J. J., Endresen, O., Grainger, R. G., Moldanova, J., Schlager, H., and Stevenson, D. S.: Transport impacts on atmosphere and climate: Shipping, Atmos. Environ., 44, 4735–4771, https://doi.org/10.1016/j.atmosenv.2009.04.059, 2010.

Federal Ministry for Digital and Transport, Inland Waterway Transport Masterplan: https://www.bmvi.de/SharedDocs/DE/Anlage/WS/masterplan-binnenschifffahrt-en.pdf?_blob=publicationFile (last access: 7 August 2023), 2019.

Federal Ministry for Digital and Transport: R&D Project 40.0399/2017 Evaluating the Energy Requirement of Inland Vessels Using Energy Efficiency Indices, Executive summary of final report no. 2252, https://www.cesni.eu/wp-content/uploads/2021/03/cesnipt_energyindex_en.pdf (last access: 7 August 2023), 2020.

Fink, L., Karl, M., Matthias, V., Oppo, S., Kranenburg, R., Kuenen, J., Moldanova, J., Jutterström, S., Jalkanen, J. P., and Majamäki, E.: Potential impact of shipping on air pollution in the Mediterranean region – a multimodel evaluation: comparison of photooxidants NO_2 and O_3, Atmos. Chem. Phys., 23, 1825–1862, https://doi.org/10.5194/acp-23-1825-2023, 2023.

Giechaskiel, B., Ntziachristos, L., Samaras, Z., Scheer, V., Casati, R., and Vogt, R.: Formation potential of vehicle exhaust nucleation mode particles on-road and in the laboratory, Atmos. Environ., 39, 3191–3198, https://doi.org/10.1016/j.atmosenv.2005.02.019, 2005.

Giechaskiel, B., Melas, A., Martini, G., Dilara, P., and Ntziachristos, L.: Revisiting Total Particle Number Measurements for Vehicle Exhaust Regulations, Atmosphere, 13, 155, https://doi.org/10.3390/atmos13020155, 2022.

Grigoriadis, A., Mamarikas, S., Ioannidis, I., Majamäki, E., Jalkanen, J.-P., and Ntziachristos, L.: Development of exhaust emission factors for vessels: A review and meta-

analysis of available data, Atmos. Environ. X, 12, 100142, https://doi.org/10.1016/j.aeaoa.2021.100142, 2021.

Gysel, N. R., Russell, R. L., Welch, W. A., and Cocker III, D. R.: Impact of Aftertreatment Technologies on the In-Use Gaseous and Particulate Matter Emissions from a Tugboat, Energy Fuels, 30, 684–689, https://doi.org/10.1021/acs.energyfuels.5b01987, 2016.

Horbanski, M., Pöhler, D., Lampel, J., and Platt, U.: The ICAD (iterative cavity-enhanced DOAS) method, Atmos. Meas. Tech., 12, 3365–3381, https://doi.org/10.5194/amt-12-3365-2019, 2019.

Hydrokontor: Erstellung eines SOBEK-River Modells für den Rhein von Iffezheim bis Pannerdense Kop als Weiterentwicklung bestehender SOBEK-RE Modelle, Projektbericht PR2278.10, 2014.

Jiang, H., Peng, D., Wang, Y., and Fu, M.: Comparison of Inland Ship Emission Results from a Real-World Test and an AIS-Based Model, Atmosphere, 12, 1611, https://doi.org/10.3390/atmos12121611, 2021.

Jiang, Y., Yang, J., Gagné, S., Chan, T. W., Thomson, K., Fofie, E., Cary, R. A., Rutherford, D., Comer, B., Swanson, J., Lin, Y., Van Rooy, P., Asa-Awuku, A., Jung, H., Barsanti, K., Karavalakis, G., Cocker, D., Durbin, T. D., Miller, J. W., and Johnson, K. C.: Sources of variance in BC mass measurements from a small marine engine: Influence of the instruments, fuels and loads, Atmos. Environ., 182, 128–137, https://doi.org/10.1016/j.atmosenv.2018.03.008, 2018.

Jonsson, Å. M., Westerlund, J., and Hallquist, M.: Size-resolved particle emission factors for individual ships, Geophys. Res. Lett., 38, L13809, https://doi.org/10.1029/2011GL047672, 2011.

Karjalainen, P., Rönkkö, T., Pirjola, L., Heikkilä, J., Happonen, M., Arnold, F., Rothe, D., Bielaczyc, P., and Keskinen, J.: Sulfur Driven Nucleation Mode Formation in Diesel Exhaust under Transient Driving Conditions, Environ. Sci. Technol., 48, 2336–2343, https://doi.org/10.1021/es405009g, 2014.

Karl, M., Jonson, J. E., Uppstu, A., Aulinger, A., Prank, M., Sofiev, M., Jalkanen, J. P., Johansson, L., Quante, M., and Matthias, V.: Effects of ship emissions on air quality in the Baltic Sea region simulated with three different chemistry transport models, Atmos. Chem. Phys., 19, 7019–7053, https://doi.org/10.5194/acp-19-7019-2019, 2019.

Kattner, L.: Measurements of shipping emissions with in-situ instruments, Universität Bremen, Bremen, https://media.suub.uni-bremen.de/handle/elib/4271 (last access: 7 August 2023), 2019.

Keuken, M. P., Moerman, M., Jonkers, J., Hulskotte, J., Denier van der Gon, H. A. C., Hoek, G., and Sokhi, R. S.: Impact of inland shipping emissions on elemental carbon concentrations near waterways in The Netherlands, Atmos. Environ., 95, 1–9, https://doi.org/10.1016/j.atmosenv.2014.06.008, 2014.

Kittelson, D. B.: Engines and nanoparticles: a review, J. Aerosol Sci., 29, 575–588, https://doi.org/10.1016/S0021-8502(97)10037-4, 1998.

Knörr, W., Heidt, C., Schmiedt, M., and Notter, B.: Aktualisierung der Emissionsberechnung für die Binnenschifffahrt und Übertragung der Daten in TREMOD, Heidelberg, ifeu – Institut für Energie- und Umweltforschung Heidelberg GmbH, INFRAS – Forschung und Beratung, https://www.umweltbundesamt.

de/publikationen/aktualisierung-tremod-mm-2019 (last access: 7 August 2023), 2013.

Korsten, L.: Technische und ökologische Auswirkungen alternativer Kraftstoffe auf die Entwicklung des zukünftigen Verkehrssystems, MS thesis, Universität Duisburg-Essen, 2018.

Krause, K., Wittrock, F., Richter, A., Busch, D., Bergen, A., Burrows, J. P., Freitag, S., and Halbherr, O.: Determination of NO$_x$ emission rates of inland ships from onshore measurements, Atmos. Meas. Tech., 16, 1767–1787, https://doi.org/10.5194/amt-16-1767-2023, 2023.

Kuittinen, N., Jalkanen, J.-P., Alanen, J., Ntziachristos, L., Hannuniemi, H., Johansson, L., Karjalainen, P., Saukko, E., Isotalo, M., Aakko-Saksa, P., Lehtoranta, K., Keskinen, J., Simonen, P., Saarikoski, S., Asmi, E., Laurila, T., Hillamo, R., Mylläri, F., Lihavainen, H., Timonen, H., and Rönkkö, T.: Shipping Remains a Globally Significant Source of Anthropogenic PN Emissions Even after 2020 Sulfur Regulation, Environ. Sci. Technol., 55, 129–138, https://doi.org/10.1021/acs.est.0c03627, 2021.

Kurtenbach, R., Vaupel, K., Kleffmann, J., Klenk, U., Schmidt, E., and Wiesen, P.: Emissions of NO, NO$_2$ and PM from inland shipping, Atmos. Chem. Phys., 16, 14285–14295, https://doi.org/10.5194/acp-16-14285-2016, 2016.

Kwasny, F., Madl, P., and Hofmann, W.: Correlation of Air Quality Data to Ultrafine Particles (UFP) Concentration and Size Distribution in Ambient Air, Atmosphere, 1, 3–14, https://doi.org/10.3390/atmos1010003, 2010.

Lack, D. A. and Corbett, J. J.: Black carbon from ships: a review of the effects of ship speed, fuel quality and exhaust gas scrubbing, Atmos. Chem. Phys., 12, 3985–4000, https://doi.org/10.5194/acp-12-3985-2012, 2012.

Li, X., Dallmann, T. R., May, A. A., Stanier, C. O., Grieshop, A. P., Lipsky, E. M., Robinson, A. L., and Presto, A. A. J. A. E.: Size distribution of vehicle emitted primary particles measured in a traffic tunnel, Atmos. Environ., 191, 9–18, 2018.

Moldanová, J., Fridell, E., Popovicheva, O., Demirdjian, B., Tishkova, V., Faccinetto, A., and Focsa, C.: Characterisation of particulate matter and gaseous emissions from a large ship diesel engine, Atmos. Environ., 43, 2632–2641, https://doi.org/10.1016/j.atmosenv.2009.02.008, 2009.

Nuszkowski, J., Clark, N. N., Spencer, T. K., Carder, D. K., Gautam, M., Balon, T. H., Moynihan, P. J. J. J. O. T. A., and Association, W. M.: Atmospheric emissions from a passenger ferry with selective catalytic reduction, J. Air Waste Manage. Assoc., 59, 18–30, https://doi.org/10.3155/1047-3289.59.1.18, 2009.

Petzold, A., Hasselbach, J., Lauer, P., Baumann, R., Franke, K., Gurk, C., Schlager, H., and Weingartner, E.: Experimental studies on particle emissions from cruising ship, their characteristic properties, transformation and atmospheric lifetime in the marine boundary layer, Atmos. Chem. Phys., 8, 2387–2403, https://doi.org/10.5194/acp-8-2387-2008, 2008.

Pillot, D., Guiot, B., Le Cottier, P., Perret, P., and Tassel, P.: Exhaust emissions from in-service inland waterways vessels, in: TAP 2016, 21st International Transport and Air Pollution Conference, J. Earth Sci. Geotech. Eng., 6, 205–225, 2016.

Pirjola, L., Pajunoja, A., Walden, J., Jalkanen, J. P., Rönkkö, T., Kousa, A., and Koskentalo, T.: Mobile measurements of ship emissions in two harbour areas in Finland, Atmos. Meas. Tech., 7, 149–161, https://doi.org/10.5194/amt-7-149-2014, 2014.

Pohl, T., Schmitz, D., Fischer, C., Heweling, G., and Weber, K.: A case-study for the investigation of inland ship emissions in real world plume dilution at the Rhine river in Duesseldorf, Germany, Int. J. Environ. Sci., 2, 258–265, 2017.

Reif, K.: Innermotorische Emissionsminderung. Dieselmotor-Management: Systeme, Komponenten, Steuerung und Regelung, Springer, https://doi.org/10.1007/978-3-8348-2179-9, 2012.

Sandradewi, J., Prévôt, A. S., Szidat, S., Perron, N., Alfarra, M. R., Lanz, V. A., Weingartner, E., and Baltensperger, U.: Using aerosol light absorption measurements for the quantitative determination of wood burning and traffic emission contributions to particulate matter, Environ. Sci. Technol., 42, 3316–3323, https://doi.org/10.1021/es702253m, 2008.

Schlaerth, H., Ko, J., Sugrue, R., Preble, C., and Ban-Weiss, G.: Determining black carbon emissions and activity from in-use harbor craft in Southern California, Atmos. Environ., 256, 118382, https://doi.org/10.1016/j.atmosenv.2021.118382, 2021.

Schwarzkopf, D. A., Petrik, R., Matthias, V., Quante, M., Yu, G., and Zhang, Y.: Comparison of the Impact of Ship Emissions in Northern Europe and Eastern China, Atmosphere, 13, 894, https://doi.org/10.3390/atmos13060894, 2022.

Schweighofer, J., and Blaauw, H.: Final Report The Cleanest Ship Project, https://doi.org/10.13140/2.1.4202.8326, 2009.

Seyler, A., Wittrock, F., Kattner, L., Mathieu-Uffing, B., Peters, E., Richter, A., Schmolke, S., and Burrows, J. P.: Monitoring shipping emissions in the German Bight using MAX-DOAS measurements, Atmos. Chem. Phys., 17, 10997–11023, https://doi.org/10.5194/acp-17-10997-2017, 2017.

Sokhi, R. S., Moussiopoulos, N., Baklanov, A., Bartzis, J., Coll, I., Finardi, S., Friedrich, R., Geels, C., Grönholm, T., Halenka, T., Ketzel, M., Maragkidou, A., Matthias, V., Moldanova, J., Ntziachristos, L., Schäfer, K., Suppan, P., Tsegas, G., Carmichael, G., Franco, V., Hanna, S., Jalkanen, J. P., Velders, G. J. M., and Kukkonen, J.: Advances in air quality research – current and emerging challenges, Atmos. Chem. Phys., 22, 4615–4703, https://doi.org/10.5194/acp-22-4615-2022, 2022.

Sugrue, R. A., Preble, C. V., Tarplin, A. G., and Kirchstetter, T. W.: In-Use Passenger Vessel Emission Rates of Black Carbon and Nitrogen Oxides, Environ. Sci. Technol., 56, 7679–7686, https://doi.org/10.1021/acs.est.2c00435, 2022.

Tang, L., Ramacher, M. O. P., Moldanová, J., Matthias, V., Karl, M., Johansson, L., Jalkanen, J. P., Yaramenka, K., Aulinger, A., and Gustafsson, M.: The impact of ship emissions on air quality and human health in the Gothenburg area – Part 1: 2012 emissions, Atmos. Chem. Phys., 20, 7509–7530, https://doi.org/10.5194/acp-20-7509-2020, 2020.

10. BImSchV.: Zehnte Verordnung zur Durchführung des Bundes-Immissionsschutzgesetzes, Verordnung über die Beschaffenheit und die Auszeichnung der Qualitäten von Kraft- und Brennstoffen, Deutschland, https://www.gesetze-im-internet.de/bimschv_10_2010/BJNR184900010.html (last access: 7 August 2023), 2010.

Uherek, E., Halenka, T., Borken-Kleefeld, J., Balkanski, Y., Berntsen, T., Borrego, C., Gauss, M., Hoor, P., Juda-Rezler, K., and Lelieveld, J. J. A. E.: Transport impacts on atmosphere and climate: Land transport, Atmos. Environ., 44, 4772–4816, https://doi.org/10.1016/j.atmosenv.2010.01.002, 2010.

Van der Gon, H. D., and Hulskotte, J.: BOP report. Methodologies for estimating shipping emissions in the Netherlands. A documentation of currently used emission factors and related activity data, https://www.tno.nl/media/2151/methodologies_for_estimating_shipping_emissions_netherlands.pdf (last access: 7 August 2023), 2010.

van der Zee, S. C., Dijkema, M. B. A., van der Laan, J., and Hoek, G.: The impact of inland ships and recreational boats on measured NO_x and ultrafine particle concentrations along the waterways, Atmos. Environ., 55, 368–376, https://doi.org/10.1016/j.atmosenv.2012.03.055, 2012.

Viana, M., Hammingh, P., Colette, A., Querol, X., Degraeuwe, B., Vlieger, I. D., and van Aardenne, J.: Impact of maritime transport emissions on coastal air quality in Europe, Atmos. Environ., 90, 96–105, https://doi.org/10.1016/j.atmosenv.2014.03.046, 2014.

von der Weiden, S. L., Drewnick, F., and Borrmann, S.: Particle Loss Calculator – a new software tool for the assessment of the performance of aerosol inlet systems, Atmos. Meas. Tech., 2, 479–494, https://doi.org/10.5194/amt-2-479-2009, 2009.

Wang, S., Zhou, K., Lu, X., Chen, H., Yang, F., Li, Q., Yang, X., and Wang, X.: Measurement of Density and Shape for Single Black Carbon Aerosols in a Heavily Polluted Urban Area, Aerosol Air Qual. Res., 21, 210162, https://doi.org/10.4209/aaqr.210162, 2021.

WHO: WHO global air quality guidelines: particulate matter ($PM_{2.5}$ and PM_{10}), ozone, nitrogen dioxide, sulfur dioxide and carbon monoxide, World Health Organization, Geneva, https://apps.who.int/iris/bitstream/handle/10665/345329/9789240034228-eng.pdf (last access: 7 August 2023), 2021.

Zhou, S., Zhou, J., and Zhu, Y.: Chemical composition and size distribution of particulate matters from marine diesel engines with different fuel oils, Fuel, 235, 972–983, https://doi.org/10.1016/j.fuel.2018.08.080, 2019.